POLITECNICO DI TORINO
Repository ISTITUZIONALE

Minimizing environmental impact in hybrid additive manufacturing: a layer-resolved decision-support tool

Original
Minimizing environmental impact in hybrid additive manufacturing: a layer-resolved decision-support tool / Catalano, A.R., Pagone, E., Eimer, E., Priarone, P.C., Settineri, L.. - In: INTERNATIONAL JOURNAL, ADVANCED MANUFACTURING TECHNOLOGY. - ISSN 0268-3768. - (2026). [10.1007/s00170-026-19025-1]

Availability:
This version is available at: 11583/3015673 since: 2026-09-17T12:24:28Z

Publisher:
Springer

Published
DOI:10.1007/s00170-026-19025-1

Terms of use:

This article is made available under terms and conditions as specified in the corresponding bibliographic description in the repository

Publisher copyright

(Article begins on next page)

29 November 2026

The International Journal of Advanced Manufacturing Technology
https://doi.org/10.1007/s00170-026-19025-1

ORIGINAL ARTICLE

Minimizing environmental impact in hybrid additive manufacturing: a layer-resolved decision-support tool

Angioletta R. Catalano[1] · Emanuele Pagone[2] · Eloïse Eimer[3] · Paolo C. Priarone[1] · Luca Settineri[1]

Received: 24 March 2026 / Accepted: 21 August 2026
© The Author(s) 2026

Abstract

Manufacturing remains a major source of greenhouse gas emissions, often locked into carbon-intensive routes. Although Additive Manufacturing (AM) improves material efficiency, its high specific energy consumption can offset environmental benefits compared to subtractive manufacturing (SM). Hybrid strategies combining AM and SM offer a promising approach, but model-based procedures to support their selection at the design stage are limited. This study presents an early-stage LCA-based decision-support framework, designed for straightforward industrial implementation, that starts from a CAD model to compare manufacturing sequences and identify those that minimize the carbon footprint (CF) within cradle-to-gate boundaries. The geometry is discretized into uniform layers, and the Solid-to-Cavity Ratio is extended to a layer-resolved form (SCR_i) scaled by process-specific impact intensities for milling and Wire Arc Additive Manufacturing (WAAM); the switching layer is selected as the one minimizing the cumulative CF over all admissible positions. Applied to three controlled benchmark geometries and the mock-up of a real industrial landing gear, the framework locates the optimal switching layer and quantifies the resulting reduction in CF, up to 61.2% relative to milling and up to 17.5% relative to WAAM, with the optimum coinciding with a single-process route in some cases. The analysis highlights that overall SCR is not always sufficient for predicting performance, as the spatial distribution of material per layer can drive impact. Sensitivity analyses considering different levels of recycled content and different electricity mixes illustrate how the framework supports exploring uncertainty and trade-offs in route selection.

Keywords Hybrid additive manufacturing · Layer-by-layer analysis · Solid-to-cavity ratio · Environmental impact assessment · Carbon footprint · Sustainable manufacturing

Nomenclature

Acronym/Symbol	Definition
CED	Cumulative Energy Demand
CF	Carbon Footprint
CI	Carbon Intensity
SEC	Specific Energy Consumption
TS	Travel Speed
WAAM	Wire Arc Additive Manufacturing
WFS	Wire Feed Speed
a	Finishing machining allowance offset distance
b	Semi-finishing machining allowance offset distance
A_p	Part cross-sectional area
A_{env}	Envelope cross-sectional area
A_1	Cross-sectional area after finishing offset
A_2	Cross-sectional area after semi-finishing offset
A_3	Reference workpiece cross-sectional area
CI_{elt}	Carbon intensity of electricity consumption

✉ Angioletta R. Catalano
angioletta.catalano@polito.it

[1] Department of Management and Production Engineering, Politecnico Di Torino, Corso Duca Degli Abruzzi 24, 10129 Turin, Italy

[2] Sustainable Manufacturing Systems Centre, Faculty of Engineering and Applied Sciences, Cranfield University, Cranfield MK43 0AL, UK

[3] Welding and Additive Manufacturing Centre, Faculty of Engineering and Applied Sciences, Cranfield University, Cranfield MK43 0AL, UK

CI_F	Carbon intensity, finishing
CI_{gas}	Carbon intensity of shielding gas
CI_{HF}	Carbon intensity, hot forming
$CI_{MatProd}$	Carbon intensity, material production
CI_R	Carbon intensity, roughing
CI_{RCA}	Carbon intensity, typical grade production (RCA approach)
CI_{Rec}	Carbon intensity, recycling
CI_{SF}	Carbon intensity, semi-finishing
CI_V	Carbon intensity, virgin grade production
CI_{WAAM}	Carbon intensity, WAAM
CI_{WD}	Carbon intensity, wire drawing
CF_H	Carbon footprint, hybrid route
CF_M	Carbon footprint, milling-based route
CF_W	Carbon footprint, WAAM-based route
DR	Deposition rate
$eSEC_W$	Electric specific energy consumption for WAAM
k	Index of the last layer produced by milling
k^*	Switching layer minimizing the cumulative carbon footprint
m_c^F	Chip mass removed during finishing
m_c^R	Chip mass removed during roughing
m_c^{SF}	Chip mass removed during semi-finishing
m_{dep}	Deposited metal mass via WAAM
$\dot{m}_{gas}$	Gas flow rate
m_p	Part mass
m_{wp}	Workpiece mass
n_L	Number of layers obtained through slicing
R	Recycled content fraction in the current supply
SCR	Solid-to-Cavity Ratio (overall)
SCR_i	Layer-resolved Solid-to-Cavity Ratio
SII	Specific Impact Intensity (generic)
SII_M^{CF}	Specific impact intensity, milling (CF metric)
SII_W^{CF}	Specific impact intensity, WAAM (CF metric)
TI	Total Impact (generic metric)
V_i	Individual layer part volume
V_L	Layer (envelope) volume
V_{env}	Envelope volume
V_p	Part volume
y_{HF}	Yield factor, hot forming
y_{WAAM}	Yield factor, WAAM
y_{WD}	Yield factor, wire drawing
ρ	Material density
ξ	Relative area increment for the finishing allowance
ψ	Relative area increment for the semi-finishing allowance
χ	Relative area increment for the roughing allowance

1 Introduction

Since the beginning of the twenty-first century, manufacturing and other industrial activities have accounted for approximately 45% of the cumulative increase in anthropogenic GHG emissions, and the industrial sector is expected to decarbonize more slowly than other sectors [1]. According to the Net Zero Roadmap of the International Energy Agency (IEA) [2], keeping the 1.5 °C goal within reach requires emissions to decline by 80% in advanced economies and by 60% in emerging market and developing economies by 2035, relative to 2022 levels. Meeting such a trajectory requires a profound transformation of production technologies. To mitigate the environmental impacts of manufacturing, selecting the most appropriate process for a given component is a critical decision point. This choice can alter the final carbon footprint by up to an order of magnitude due to variations in material yield and energy demand [3], as well as post-processing requirements and process-specific qualification considerations [4]. Decision-support tools that integrate life cycle assessment (LCA), particularly in the early design stages, are therefore essential to guide manufacturers toward sustainable choices [5].

In the literature, two main research streams address this need. The first concerns multi-criteria decision-making frameworks. Wortmann et al. [6] consider geometry, material properties, production cost, and environmental impact, integrating AM feasibility assessment into early design stages in line with design for additive manufacturing (DFAM) principles. Their method uses expert knowledge to classify parts based on multiple attributes (shape, application, volume, tolerances, surface form, material properties, and conventional producibility), evaluates attribute relationships through a consistency matrix, and visualizes part classes in a multidimensional space to match them with suitable additive or subtractive manufacturing processes. Schuhmann et al. [7] apply the Analytic Hierarchy Process (AHP), structuring 31 criteria into seven categories. Their framework, validated through two industrial case studies, illustrates how rankings of manufacturing options can shift depending on the prioritization of objectives. Another study by Priarone et al. [8] combines a 'cradle-to-gate' life cycle assessment (LCA), i.e., covering all stages from raw

material extraction to the finished part, with the TOPSIS multi-criteria decision-making (MCDM) method to evaluate WAAM and milling for three components of different geometries and materials, showing that WAAM offers greater advantages when environmental sustainability is prioritized, although trade-offs with time, cost, and quality remain. The second stream focuses on geometry-driven indicators for decision-making. Wang et al. [9] propose a similarity-search methodology using shape descriptors and mathematical models of essential geometric features, combined with material information, to match new designs with previously manufactured parts. This approach can support process recommendations that reflect both geometry and material constraints, although it requires substantial data input or domain expertise. Other studies have incorporated component geometry into decision analysis through indicators such as the part volume ratio [10] and the shape-factor K [11], used as predictors of process efficiency. Among these, the Solid-to-Cavity Ratio (SCR), defined as the ratio between the volume of a part and its enveloping volume, has emerged as one of the most effective geometry-based metrics. Priarone et al. [12] demonstrate that Electron Beam Melting (EBM) is advantageous for geometries with low SCR, whereas subtractive manufacturing is more efficient for simpler parts. Ingarao and Priarone [13] extend this by including cost and use-phase impacts, identifying SCR and the lightweight ratio as critical break-even metrics for selecting between EBM and turning.

Comparative studies across additive and subtractive manufacturing indicate that AM often outperforms SM when material utilization in subtractive processes is low, particularly when scrap rates exceed 70% or when the recyclability of removed material is limited [14]. In contrast, bulk geometries, stringent surface quality requirements, and high-volume production generally require SM. Within this broader comparative landscape, process-specific investigations have highlighted the role of individual technologies. Wire Arc Additive Manufacturing (WAAM) has emerged as a promising method to produce large metallic parts, often achieving lower cost and carbon footprint than powder-based AM [15]. Kokare et al. [16] and Reis et al. [15] confirm the superior material efficiency and lower environmental footprint of WAAM compared to milling, while noting that post-processing can influence cost competitiveness.

Hybrid manufacturing, which combines AM and SM in a single workflow, has also been examined. Liu et al. [3] show that additive-subtractive hybrid manufacturing (ASHM) is particularly suitable for weight-sensitive applications, while conventional subtractive manufacturing is more efficient when weight savings are not relevant. Liu et al. [17] report that hybrid DED-CNC reduces environmental impact by 53% compared to CNC alone, and Liu et al. [18] show that Hybrid Deposition and Micro Rolling (HDMR) emits 14 times less CO_2 than forging. These studies highlight the potential of hybrid strategies to lower environmental burdens under specific conditions. However, their findings remain limited to case-specific investigations, not providing a generalized framework for process selection across diverse geometries and applications. The present paper builds on these contributions by developing a systematic, layer-resolved approach that moves from individual case studies toward a more generalizable decision-support perspective and addresses the absence of tools applicable at the early design stage.

A synthesis of these comparative studies is presented in Table 1, which details the processes, materials, case study geometries, LCA boundaries, and assessment focus. The table highlights that most contributions analyze single geometries and assess entire parts manufactured exclusively by one process, predominantly focusing on titanium alloys and relying on global metrics such as the overall SCR. These approaches are unable to capture how local material distribution or layer-specific characteristics influence environmental performance, and they overlook the possibility of assigning different processes to different regions of a component. To the best of the authors' knowledge, no existing framework applies a spatially resolved, CAD-driven LCA-based analysis capable of identifying where and when switching between additive and subtractive strategies becomes advantageous.

The objective of this study is to develop a decision-support modeling framework that identifies the manufacturing route, or sequence of routes, which minimizes cradle-to-gate greenhouse gas emissions directly from a CAD model. Unlike existing approaches, the method does not require geometric feature cataloguing or detailed LCA expertise. By relying solely on the CAD geometry and a material-process database, it provides rapid environmental estimates to support early-stage process selection. The framework is conceived as a screening-level tool aimed at comparing alternative manufacturing routes. Although grounded in process-specific and geometry-resolved formulations, it does not aim to replace a full ISO-compliant LCA. Rather, it supports preliminary design and manufacturing decisions by enabling structured comparisons prior to detailed LCA studies.

The framework compares additive, subtractive, and hybrid strategies for metal components of low to medium geometric complexity. The SCR descriptor, the cradle-to-gate system boundary and the milling and WAAM impact inventories on which it relies build on previous work by the authors [8, 12, 13, 25]. What the present study introduces is the extension of the SCR to a layer-resolved form: in contrast to component-level comparisons, including the

Table 1 Research studies comparing additive, subtractive, and hybrid manufacturing processes, detailing the materials investigated, case study geometries, life-cycle assessment boundaries, and focus of the analysis

Reference	Compared processes		Material	Case study	Analysis boundaries	Assessment
Kokare et al. [16]	WAAM, SLM	Milling	Steel (ER70)	Marine propeller	Cradle to gate	Environmental and cost
Kokare et al. [16]	WAAM, SLM	Milling	Steel (ER70)	Gear geometry	Cradle to gate	Environmental and cost
Reis et al. [15]	WAAM	Milling	Steel (ER70)	Cylinder geometry	Cradle to gate	Environmental
Reis et al. [15]	WAAM	Milling	Steel (ER70)	S-shaped geometry	Cradle to gate	Environmental
Priarone et al. [8]	WAAM	Milling	Steel (ER70s-6)	Cantilever beam	Cradle to gate	Environmental, cost, quality, time
Priarone et al. [8]	WAAM	Milling	Aluminum (AA2319)	Aerospace frame	Cradle to gate	Environmental, cost, quality, time
Priarone et al. [8]	WAAM	Milling	Titanium (Ti-6Al-4V)	Aerospace bracket	Cradle to gate	Environmental, cost, quality, time
Campatelli et al. [19]	WAAM	Milling	EN S235JR steel	NACA blade	Cradle to gate + End of Life	Environmental
Liu et al. [18]	HDMR	Forging	Titanium (Ti-6Al-4V)	Cross-shaped geometry	Cradle to gate	Environmental
Le and Paris [20]	EBM	Conventional machining	Aluminum (AA2319)	Aerospace frame	Cradle to gate	Environmental
Le and Paris [20]	EBM	Conventional machining	Titanium (Ti-6Al-4V)	Lightweight part	Cradle to gate	Environmental
Lyons et al. [21]	EBM	Milling	Titanium (Ti-6Al-4V)	Knee implant	Cradle to gate + End of Life	Environmental
Priarone et al. [12]	EBM	Conventional machining	Titanium (Ti-6Al-4V)	Three geometries with different SCR	Cradle to gate + End of Life	Environmental
Ingarao and Priarone [13]	EBM	Turning	Titanium (Ti-6Al-4V)	Axisymmetric geometry	Cradle to grave	Environmental and cost
Paris et al. [11]	EBM	Milling	Titanium (Ti-6Al-4V)	Aeronautical turbine	Cradle to grave	Environmental
Priarone et al. [22]	EBM	Conventional machining	Titanium (Ti-6Al-4V)	Aerospace bracket	Cradle to grave	Environmental
Mecheter et al. [23]	DMLS	Conventional machining	Steel (316L)	Cubic thin-walled structure	Cradle to gate	Environmental and cost
Mecheter et al. [23]	DMLS	Conventional machining	Steel (316L)	Grooved thin-walled structure	Cradle to gate	Environmental and cost
Mecheter et al. [23]	DMLS	Conventional machining	Steel (316L)	Shaft holder	Cradle to gate	Environmental and cost
Liu et al. [17]	DED	Conventional machining	Steel (316L)	Turbine blade	Cradle to gate	Environmental
Serres et al. [24]	CLAD®	Conventional machining	Titanium (Ti-6Al-4V)	Mechanical part	Cradle to gate + End of Life	Environmental
Liu et al. [3]	Metal laser direct deposition	Milling	Steel (316L)	Bearing bracket	Cradle to grave	Environmental

CLAD, construction laser additive directe (in French), *DED* directed energy deposition, *DMLS* direct metal laser sintering, *EBM* electron beam melting, *HDMR* hybrid deposition and micro rolling, *SLM* selective laser melting, *WAAM*, wire arc additive manufacturing

authors' own, each layer along the build direction is evaluated separately, so that the build height at which switching from machining to WAAM minimizes the cumulative footprint can be identified. Resolving the comparison per layer, in turn, required the machining allowances to be parametrized layer-wise, so that the material deposited and removed is tracked at each height. On this basis, the model shows how spatial material distribution within the envelope volume drives environmental trade-offs and explains inconsistencies reported in component-level LCAs. The remainder of the paper is organized as follows: Section 2 presents the methodology, formalizing the layer-resolved SCR metric, the analytical model, and the case-study setup and data inventory; Section 3 discusses the results; and Section 4 summarizes the conclusions and future work.

2 Methodology

This section presents the methodological framework developed in this study. SubSection 2.1 introduces the geometric background underpinning the approach, focusing on the Solid-to-Cavity Ratio (SCR) and its layer-resolved extension, which together provide the conceptual foundation for describing both the global occupancy and the layer-wise distribution of material within the envelope volume. SubSection 2.2 formalizes the modeling framework, while SubSection 2.3 describes the case-study setup and data inventory, including the material and manufacturing-process data used for the layer-resolved assessment.

2.1 Solid-to-Cavity ratio (SCR) and material layout: theoretical background and conceptual foundation

The Solid-to-Cavity Ratio (SCR) can be defined as the ratio between the volume of a part (V_p) and the volume of the envelope that contains it (V_{env}). This ratio provides a measure of how much of the available bounding volume is effectively occupied by the component. Formally, SCR is a volumetric parameter, while also serving as a geometry-based indicator, as it reflects the global material occupancy within the bounding envelope. This dual nature explains why SCR is widely used in comparative assessments of manufacturing performance, particularly when analyzing material efficiency and geometric utilization across different process routes. This parameter is often used in comparative studies that evaluate the environmental impact of different manufacturing processes, particularly when contrasting additive manufacturing and subtractive manufacturing techniques. In many cases, components with lower SCR values are found to be more efficiently produced using additive methods [13, 25]. This is because, for the same part produced, the subtractive route considered in this study starts from a full-size workpiece and removes large amounts of material, whereas additive manufacturing deposits material only where needed, thereby generally reducing material waste and energy demand.

Liu et al. [3] showed that, below a critical SCR threshold, additive manufacturing (AM) is preferable to subtractive manufacturing (SM) in terms of energy consumption, whereas above that threshold SM becomes more efficient. Priarone and Ingarao [25], building on the definition originally proposed by Morrow et al. [26], considered the SCR as a mass-based ratio and used it to quantify both the geometric complexity of a part and the raw-material efficiency of turning operations. They observed that low SCR values are associated with large amounts of machined-off material in SM, but correspondingly small material inputs in AM. Paris et al. [11] related shape complexity to manufacturing decisions by introducing a dimensionless shape factor, defined as the ratio between the initial blank volume and the final part volume. Although distinct from SCR, this indicator captures the amount of material removal and therefore reflects a similar geometric rationale for process selection.

Most existing comparisons rely on an 'overall SCR' value, calculated for the entire part. However, this approach (i.e., entirely additive versus entirely subtractive) can be limiting, especially when hybrid manufacturing strategies are considered. In this study, hybrid manufacturing is intended as the sequential use of subtractive and additive processes, such as depositing additional features onto a machined substrate. To overcome the limitations of such comparisons, the proposed methodology introduces a discretized, layer-by-layer analysis. Inspired by the intrinsic nature of AM processes, this approach evaluates the environmental impact associated with each individual layer when produced additively or in a subtractive way. This enables the identification of candidate layers at which the relative environmental preferability of the two processes changes and provides the layer-resolved information required to determine the optimal switching position. In extending previous methodologies [8, 19], the present study combines each layer-resolved SCR value, here denoted as SCR_i, with the process-dependent impact intensity associated with the manufacturing route applied at that layer.

This concept can be formalized through an analytical expression. By dividing both the part volume and its envelope into n_L layers, a distinct SCR_i can be calculated for each layer: by construction, the overall SCR of the part is the arithmetic mean of all individual SCR_i values, as shown in Eq. 1. It is worth noting that this equivalence (between the overall SCR and the arithmetic mean of the layer-resolved SCR_i) holds under the assumption of uniform slicing thickness and, therefore, constant envelope volume per layer. In

fact, under these conditions, each layer contributes equally to the overall envelope volume, making the arithmetic mean a valid aggregation. Different slicing strategies or non-uniform layer volumes would require a weighted formulation.

$$\mathrm{SCR} = \frac{\mathrm{V_p}}{\mathrm{V_{env}}} = \frac{\mathrm{V_1} + \mathrm{V_2} + \cdots + \mathrm{V_{n_L}}}{\mathrm{V_{env}}} = \frac{\mathrm{SCR_1} \cdot \mathrm{V_L} + \mathrm{SCR_2} \cdot \mathrm{V_L} + \cdots + \mathrm{SCR_{n_L}} \cdot \mathrm{V_L}}{\mathrm{n_L} \cdot \mathrm{V_L}} = \frac{\mathrm{V_L} \cdot (\mathrm{SCR_1} + \mathrm{SCR_2} + \cdots + \mathrm{SCR_{n_L}})}{\mathrm{n_L} \cdot \mathrm{V_L}} = \frac{\sum_{i=1}^{n_L} \mathrm{SCR_i}}{\mathrm{n_L}} \quad (1)$$

where:

- V_p is the part volume;
- V_{env} is the bounding envelope volume;
- n_L is the number of layers obtained through slicing;
- V_L is the volume of each identical layer derived from slicing V_{env};
- V_i are the individual layer volumes of the part, from $i=1$ to $i=n_L$;
- SCR_i are the layer-resolved SCR values.

When assigning an impact intensity to each layer-resolved SCR_i, two situations may arise depending on the selected manufacturing processes. If the same impact intensity, for example an identical environmental impact per unit of material, is applied uniformly across all layers, the overall SCR remains a valid and sufficient comparative metric. Conversely, when impact intensities vary across layers, as is typical in hybrid manufacturing scenarios where subtractive operations affect the lower layers while additive deposition governs the upper ones, the overall SCR becomes inadequate to accurately represent geometry-dependent impacts along the build height. In such cases, a layer-resolved evaluation provides a more detailed and meaningful basis for comparing alternative manufacturing strategies.

Moreover, the same geometric feature can generate different impacts not only depending on the selected process but also depending on the envelope volume in which it is contained. Figure 1 illustrates this concept by comparing the same feature embedded within two different envelope volumes. In the highlighted slice of *Part A* in Fig. 1, the envelope is smaller, and the ratio between the slice volume of the part and its corresponding envelope layer ($SCR_{i\,A}$) is higher than that observed for *Part B*, where the same part slice is placed in a larger envelope ($SCR_{i\,B}$). If a subtractive process is considered, producing the same feature in a larger envelope requires more feedstock material to be initially produced and subsequently removed, thereby increasing the associated impact. These considerations contribute to defining the environmental relevance of each layer within the component. For this reason, while the overall SCR remains a useful indicator, it is not sufficient on its own to fully describe the geometric complexity and material distribution of a part.

2.2 Modeling framework

Figure 2 illustrates the workflow of the proposed decision-support framework, highlighting both the user-defined inputs and the sequential computational steps leading to the identification of the preferred manufacturing route. The primary goal is to start with the CAD file and achieve a layer-by-layer environmental impact mapping, to determine whether and when to switch from the subtractive to the additive approach. The workflow comprises four main steps:

- *Step A – Slicing*: the initial input is the component CAD file (e.g., STEP or STL format), which provides detailed geometric and spatial layout information. Using a slicing procedure, the part is discretized into layers of uniform thickness. Thinner layers yield higher-resolution analyses but increase computational effort and processing time, with diminishing returns beyond a certain threshold. In this research, a planar slicing approach along the vertical axis (here indicated as the Z-axis, conventionally defined as the growth direction in AM) is adopted,

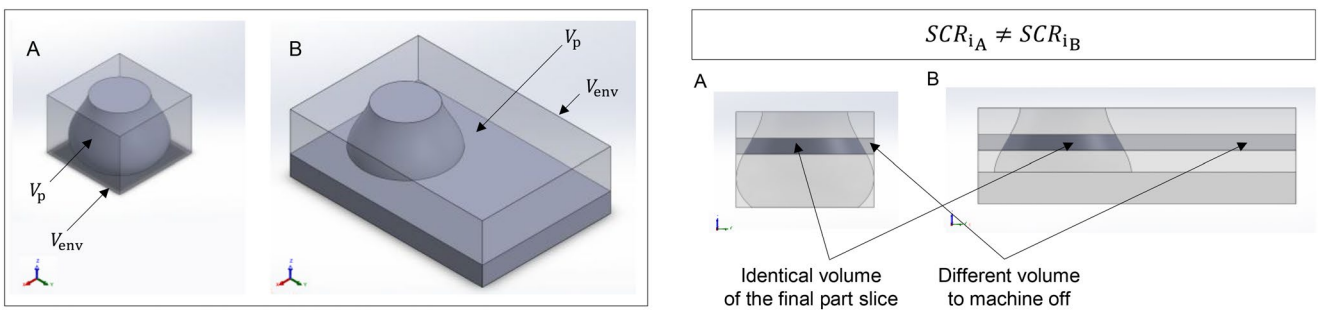


Fig. 1 Generic components *A* and *B* with identical features placed in different envelope volumes, resulting in different material distributions and corresponding SCR_i values

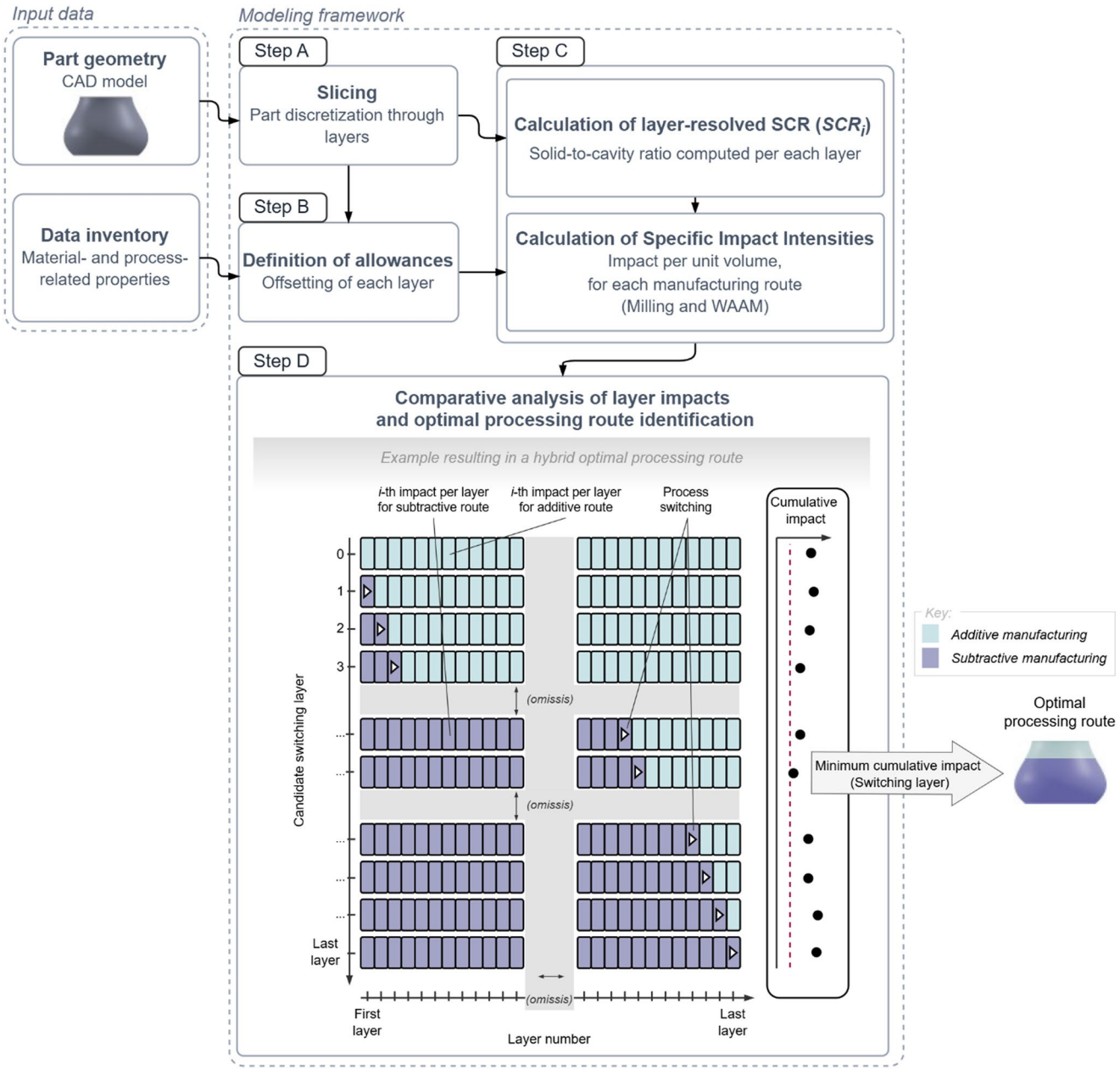


Fig. 2 Workflow illustrating the methodology steps, from CAD input to identification of the optimal processing route

which is typical for standard three-axis manufacturing processes.

- *Step B – Definition of allowances*: each sliced layer undergoes a user-defined offsetting operation, representing the process-dependent allowances defined by the user and required for subsequent machining operations (roughing, semi-finishing, and finishing).
- *Step C – Calculation of SCR_i and Specific Impact Intensity evaluation*: Before calculating the layer-resolved SCR_i values, a common geometric reference envelope is defined to ensure a consistent geometric basis for comparison across the considered processing routes. Among the feasible initial volumes associated with the alternative manufacturing strategies, the maximum bounding volume is selected and adopted as the common reference envelope. This corresponds to the largest initial stock from which material is removed or transformed to obtain the final component. In the present study, the purely subtractive route starts from a parallelepiped workpiece, which represents the largest feasible initial volume and is therefore adopted as the reference envelope for all routes, including WAAM. If, instead, two DED processes are compared (e.g., powder-based and wire-based DED),

the largest feasible bounding volume associated with their respective near-net-shape configurations is selected to maintain geometric consistency in the SCR calculation. Once the individual layer volumes (or cross-sectional areas) are established, an SCR for each layer (SCR_i) is calculated. Each layer contribution is then evaluated by combining the corresponding SCR_i value with the process-specific impact intensity associated with the selected manufacturing processes (in this study, milling and WAAM).

- *Step D – Comparative analysis of layer impacts and optimal processing route identification*: the impacts for each individual layer, mapped along the Z-axis for both milling and WAAM, are overlaid and comparatively analyzed. This comparison identifies whether iso-impact Z-levels are present, i.e., Z-levels at which the impacts of the two processes are equal and which may mark a reversal in their relative environmental preferability, indicating the potential for a hybrid processing route, and providing the basis for locating the optimal switching point from subtractive to additive manufacturing. The optimal manufacturing route is the one that minimizes the total impact, which is obtained by summing the contributions from the starting point (Z = 0) to the final layer. For hybrid routes, cumulative impact combines subtractive contributions up to the switching point and additive contributions thereafter. To identify the optimal switching point, particularly when several iso-impact levels exist along the Z-axis, the following procedure is adopted. Starting from the fully additive route, the subtractive stage is progressively extended one layer at a time: each layer is taken in turn as the last one produced subtractively, with all the layers above it produced additively, and the cumulative impact of the resulting route is computed as described above. One cumulative value is thus obtained for every candidate, and the lowest among them identifies the optimal switching point. Since the procedure spans every candidate, from no layer milled to all layers milled, the two single-process routes are already included as its extreme values.

Further details on the computational implementation of these steps are provided in Sections 2.2.1 to 2.2.3.

2.2.1 Parametrization for allowances definition (Step B)

WAAM typically requires finishing operations by material removal. To ensure a consistent comparison among the additive and subtractive processes considered in this section, the following assumptions were made:

(i) in the WAAM scenario, the deposited material includes the volumes that must be removed during semi-finishing and finishing machining operations;
(ii) the subtractive scenario is assumed to include roughing, semi-finishing, and finishing operations;
(iii) the same amounts of material to be removed during semi-finishing and finishing apply in both approaches.

Moreover, to make the model more generally applicable, if powder-based AM processes are considered, only the finishing allowance would be included and assumed to be identical for both wire-based and powder-based approaches. This assumption is supported by the higher geometric accuracy typically achieved by powder-based processes, which generally results in reduced post-deposition machining requirements compared to wire-based approaches [27]. All the allowances are defined here in such a way that the equations for environmental impact assessment can be parameterized based on them. Specifically, two offset distances, a and b (Fig. 3), are introduced. The former delineates the *finishing* machining allowance from the perimeter of the cross-sectional area of the part (A_p, Fig. 3), whereas the latter, measured from the previous offset contour, identifies the *semi-finishing* machining allowance. Consequently, the corresponding areas A_1 and A_2 are defined, as illustrated in Fig. 3a.

Each allowance is applied sequentially to the geometry resulting from the previous stage. Area A_1 is then expressed as the original cross-sectional area A_p increased by the relative area increment ξ (Eq. 2), while area A_2 is expressed as area A_1 further increased by the relative increment ψ (Eq. 3).

$$A_1 = A_p \cdot (1 + \xi) \tag{2}$$

$$A_2 = A_p \cdot (1 + \xi)(1 + \psi) \tag{3}$$

Consequently, the material removed in the finishing stage corresponds to $A_1 - A_p$, whereas in the semi-finishing it corresponds to $A_2 - A_1$. To parameterize the material removed during roughing, area A_3 is obtained by further expanding area A_2 by the relative increment χ (Eq. 4).

$$A_3 = A_p \cdot (1 + \xi)(1 + \psi)(1 + \chi) \tag{4}$$

The roughing operation thus corresponds to the removal of material defined by $A_3 - A_2$, where A_3 represents the cross-sectional area of the reference workpiece, obtained by expanding the reference envelope cross-section (A_{env}) by the offsets a and b, corresponding respectively to the finishing and semi-finishing allowances (Fig. 3). This ensures that even in sections where the component fully occupies

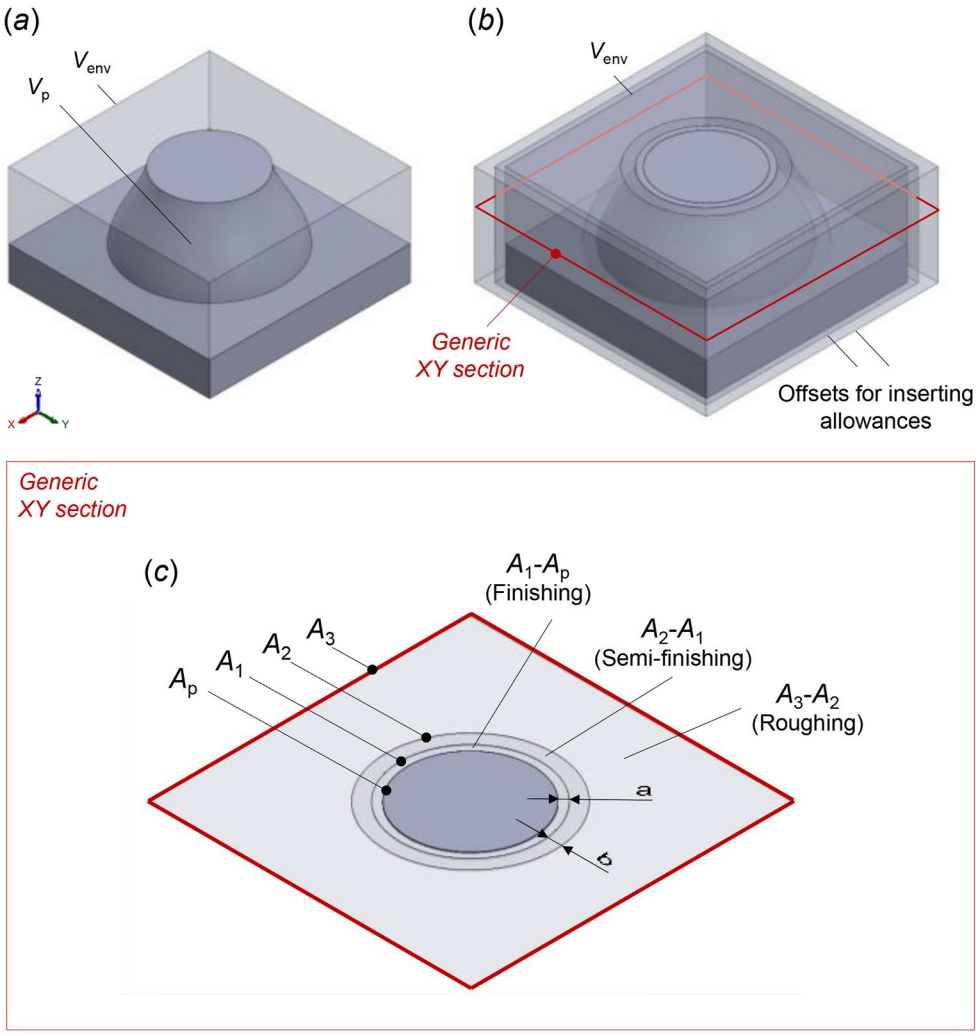


Fig. 3 Schematic representation of **a** part and envelope volumes, **b** offsetting for insertion of allowances, **c** part cross-sectional view showing *a*- and *b*-offsets and the corresponding allowance areas.

the envelope volume, sufficient allowance remains to perform finishing and semi-finishing operations.

It is worth remarking that unlike ξ and ψ, the parameter χ depends not only on the component geometry but also on its relation to the reference envelope volume surrounding the part, thus affecting the mass of the workpiece to be processed. The coefficients ξ, ψ and χ are computed directly from the offset geometries, allowing the formulation to naturally account for both section shape and envelope size. This hierarchical parameterization is preserved throughout the subsequent impact formulation.

2.2.2 Process-related intensity assignments for total impact assessment (Step C)

In general terms, an impact model, whether environmental, economic, or otherwise, can be expressed according to Eq. 5:

$$TI = V_p \cdot SII \tag{5}$$

where:

- *TI* represents the Total Impact, defined according to a selected metric (e.g., $CO_{2\ eq}$ emissions and Cumulative Energy Demand (CED) for environmental impact or total cost for the economic one).
- V_p is the volume of the examined part.
- *SII* (Specific Impact Intensity) is the impact per unit volume for the considered metric.

When the part is sliced, its total volume V_p can be expressed as the sum of the volumes of individual layers (Eq. 1). Substituting this into Eq. 5, the *TI* becomes the sum of the layer-wise contributions, as shown in Eq. 6:

$$TI = \sum_{i=1}^{n_L} (V_i \cdot SII_i) = \sum_{i=1}^{n_L} (V_L \cdot SCR_i \cdot SII_i) \tag{6}$$

In this expression, V_L is the (constant) volume of each layer, SCR_i is the Solid-to-Cavity Ratio at layer i, and SII_i is the Specific Impact Intensity associated with the manufacturing process applied at that layer.

These layers are computational slices, whose thickness is set by the slicing step adopted for the analysis and is not required to match that of a deposited bead. Each is treated as independent of the others for the purpose of the impact assessment, so that the thermal history of the deposit is not represented, consistently with the objective of supporting an early-stage comparison between routes rather than simulating the process. This formulation enables detailed and geometry-resolved evaluation of environmental performance, by aggregating process-specific contributions in a cumulative metric. Once the impact metric is selected, such as CED, or $CO_{2\ eq}$ emissions as in the present study, it is necessary to define all contributing factors within a life-cycle perspective.

The adopted framework, applied to both milling and WAAM, captures material flows and $CO_{2\ eq}$ emissions across all the cradle-to-gate stages. Moreover, even though the equations presented in the following focus exclusively on $CO_{2\ eq}$, equivalent formulations can be applied to other impact metrics when the corresponding metric-related data are available. The value of SII_i is material- and process-dependent and must be derived for each manufacturing route considered. The following subsections formalize the process-specific impact models for WAAM and milling, from which the corresponding SII_i expressions are obtained. These SII_i functions constitute the link between the layer geometry and the environmental intensity of each process, enabling the layer-wise formulation introduced in Eq. 6.

Although the formulation presented below distinguishes pure additive and subtractive routes, it is worth noting that, in industrial practice, WAAM-based manufacturing employed to build a component from scratch (i.e., not in a repair scenario) always requires a conventionally manufactured substrate. Depending on the application, this substrate may or may not remain part of the final product. According to the modeling framework adopted in this study, practical WAAM processes in which the substrate is assumed to remain part of the final product correspond to the hybrid routes presented here: the layers up to the substrate thickness are treated as subtractive, while all subsequent layers are treated as additive. Consequently, the switching point of the hybrid route is determined by the physical substrate thickness.

The transition between the subtractive and the additive stage may in practice call for additional operations such as stress relief, substrate preheating or specific surface preparation. These are outside the scope of the model, since their necessity and extent depend on the part, the material and the equipment available, and on whether the two stages are carried out on the same machine or in separate facilities, none of which is defined at the stage the tool is intended to support. The framework is intentionally formulated so that such contributions can be incorporated as additional route-dependent penalty terms whenever they are known.

WAAM-related SII for Carbon Footprint

In this study, the *TI* is evaluated in terms of $CO_{2\ eq}$ emissions associated with the manufactured part, that is the functional unit of the cradle-to-gate assessment. For consistency throughout the manuscript, such total emissions will be referred to as the *Carbon Footprint* (CF), expressed either in kg/part or simply kg. The term *Carbon Intensity* (CI), by contrast, denotes the emissions normalized to the relevant reference quantity, for example kg per kWh for electricity consumption or kg per kilogram of argon consumed for shielding gas usage.

The cradle-to-gate boundary adopted for the WAAM route comprises material production, hot forming, wire drawing and deposition, followed by the semi-finishing and finishing machining operations. On this basis, the CF associated with WAAM-based manufacturing, denoted as CF_W, is quantified in Eq. 7:

$$\begin{aligned} CF_W = m_{dep} \cdot [y_{WAAM} \cdot [(CI_{MatProd} + CI_{HF}) \cdot y_{WD} \cdot y_{HF} + \\ CI_{WD} \cdot y_{WD}] + CI_{WAAM}] + CI_{SF} \cdot m_c^{SF} + CI_F \cdot m_c^F \end{aligned} \quad (7)$$

where:

- m_{dep} is the deposited metal mass via WAAM (kg);
- y_{WAAM}, y_{WD}, and y_{HF}, are the yield factors (here intended as input/output material ratio) for WAAM, wire drawing, and hot forming, respectively;
- $CI_{MatProd}$ is the carbon intensity for material production, either from virgin sources or including recycled material (kg of CO_2 per kg of produced material);
- CI_{WAAM} is the carbon intensity associated with WAAM (kg of CO_2 per kg of deposited material);
- CI_{WD} and CI_{HF} are the carbon intensities associated with wire drawing and hot forming, respectively (kg of CO_2 per kg of material entering each process);
- CI_{SF} and CI_F are the carbon intensity values for semi-finishing and finishing operations, respectively (kg of CO_2 per kg of removed material);
- m_c^{SF} and m_c^F are the masses removed as chips during semi-finishing and finishing operations, respectively (kg).

The expression is constructed by tracing the material flow backwards, from the mass actually deposited to the raw material that has to be produced in order to obtain it. Each yield factor allows quantifying the material lost at the

corresponding stage, so that the mass entering every step upstream is progressively larger than the mass leaving it.

It is worth noting that the term relating to the *CI* of WAAM can be further expressed by specifying the contribution of emissions due to the use of both electricity and shielding gas during deposition, and can be expressed as follows:

$$\mathrm{CI_{WAAM}} = \frac{\mathrm{CI_{gas}} \cdot \dot{\mathrm{m}}_{\mathrm{gas}}}{\mathrm{DR}} + \mathrm{eSEC_W} \cdot \mathrm{CI_{elt}} \tag{8}$$

where:

- CI_{gas} is the carbon intensity of the shielding gas (kg of CO_2 per kg of gas);
- $\dot{m}_{gas}$ is the gas flow rate (kg of gas per hour);
- DR is the deposition rate (kg of deposited mass per hour);
- $eSEC_W$ is the electric Specific Energy Consumption during WAAM (kWh per kg of deposited mass);
- CI_{elt} is carbon intensity for electricity consumption (kg of CO_2 per kWh).

According to the allowance parametrization introduced in Section 2.2.1, the deposited mass (Eq. 9) and the chip masses for finishing and semi-finishing (Eqs. 10–11) are expressed as follows:

$$\mathrm{m_{dep}} = \mathrm{m_p} \cdot (1+\xi)(1+\psi) \tag{9}$$

$$\mathrm{m_c^F} = \mathrm{m_p} \cdot \xi \tag{10}$$

$$\mathrm{m_c^{SF}} = \mathrm{m_p} \cdot (1+\xi)\psi \tag{11}$$

Substituting Eqs. 9–11 into Eq. 7, and expressing part mass as the product of its volume and density ($m_p = V_p \cdot \rho$), yields the parameterized expression for WAAM-based CF:

$$\begin{aligned}\mathrm{CF_W} = \mathrm{V_p} \cdot \rho \cdot \{(1+\xi)(1+\psi) \cdot [\mathrm{y_{WAAM}} \cdot \\ [(\mathrm{CI_{MatProd}} + \mathrm{CI_{HF}}) \cdot \mathrm{y_{WD}} \cdot \mathrm{y_{HF}} + \mathrm{CI_{WD}} \cdot \mathrm{y_{WD}}] + \\ \mathrm{CI_{SF}} \cdot (1+\xi)\psi + \mathrm{CI_F} \cdot \xi\}\end{aligned} \tag{12}$$

This expression corresponds to the general impact formulation given in Eq. 7, where the product $V_p \cdot SII$ defines the total metric impact. The term that multiplies V_p represents the metric-Specific Impact Intensity for WAAM, SII_W^{CF}. By applying the slicing strategy introduced earlier, the total CF for WAAM is expressed in layer-wise form as:

$$\mathrm{CF_W} = \sum_{\mathrm{i}=1}^{\mathrm{n_L}} \mathrm{V_L} \cdot \mathrm{SCR_i} \cdot \mathrm{SII_{i,W}^{CF}} \tag{13}$$

Here, $SII_{i,W}^{CF}$ denotes the specific impact intensity associated with layer i, where the allowance coefficients (ξ_i, ψ_i) are also layer-specific. The corresponding expression becomes:

$$\begin{aligned}\mathrm{SII_{i,W}^{CF}} = \rho \cdot \{(1+\xi_\mathrm{i})(1+\psi_\mathrm{i}) \cdot \\ [(\mathrm{CI_{MatProd}} + \mathrm{CI_{HF}}) \cdot \mathrm{y_{WD}} \cdot \mathrm{y_{HF}} + \mathrm{CI_{WD}} \cdot \mathrm{y_{WD}}] + \\ \mathrm{CI_{SF}} \cdot (1+\xi_\mathrm{i})\psi_\mathrm{i} + \mathrm{CI_F} \cdot \xi_\mathrm{i}\}\end{aligned} \tag{14}$$

Milling-related SII for Carbon Footprint

The cradle-to-gate boundary adopted for the milling route comprises material production and hot forming, followed by the roughing, semi-finishing and finishing machining operations. On this basis, the CF associated with milling-based manufacturing, denoted as CF_M, is quantified in Eq. 15:

$$\mathrm{CF_M} = (\mathrm{CI_{MatProd}} + \mathrm{CI_{HF}}) \cdot \mathrm{m_{wp}} \cdot \mathrm{y_{HF}} + \mathrm{CI_R} \cdot \mathrm{m_c^R} + \mathrm{CI_{SF}} \cdot \mathrm{m_c^{SF}} + \mathrm{CI_F} \cdot \mathrm{m_c^F} \tag{15}$$

where:

- $CI_{MatProd}$ is the carbon intensity for material production, either from virgin sources or including recycled material (kg of CO_2 per kg of produced material);
- CI_{HF} is the carbon intensity associated with hot forming (kg of CO_2 per kg of material entering the process);
- m_{wp} is the mass of the workpiece entering the machining stage (kg);
- y_{HF} is the yield factor (input/output material ratio) associated with the hot forming process;
- CI_R, CI_{SF} and CI_F are the carbon intensity values referred to the removed material for roughing, semi-finishing, and finishing, respectively (kg of CO_2 per kg of removed material);
- m_c^R, m_c^{SF} and m_c^F are the masses of chips removed during roughing, semi-finishing, and finishing, respectively (kg).

The expression follows the same logic as Eq. 7, traced backwards from the workpiece to the raw material that has to be produced to obtain it. Only one yield factor is involved, since the workpiece reaches the machine tool directly after hot forming. The machining terms are instead applied to the material actually removed at each stage.

Integrating the allowance parameterization, the workpiece mass is defined as:

$$\mathrm{m_{wp}} = \mathrm{m_p} \cdot (1+\xi)(1+\psi)(1+\chi) \tag{16}$$

As anticipated, the masses of chips to be removed during finishing (m_c^F) and semi-finishing (m_c^{SF}) are the same as those defined for the WAAM-based approach, in order to ensure consistent comparability between the two processes.

In addition, the subtractive route includes a roughing operation, whose removed chip mass is expressed as:

$$m_c^R = m_p \cdot (1+\xi)(1+\psi)\chi \tag{17}$$

By substituting these expressions into the general CF equation (Eq. 15) and representing the part mass as the product of volume and density ($m_p = V_p \cdot \rho$), the parameterized CF for milling becomes:

$$\begin{aligned} CF_M = V_p \cdot \rho \cdot [(CI_{MatProd} + CI_{HF}) \cdot y_{HF} \cdot (1+\xi)(1+\psi)(1+\chi) + \\ CI_R \cdot (1+\xi)(1+\psi)\chi + CI_{SF} \cdot (1+\xi)\psi + CI_F \cdot \xi] \end{aligned} \tag{18}$$

As in WAAM, the impact can be expressed in a layer-wise form using the slicing approach:

$$CF_M = \sum_{i=1}^{n_L} V_L \cdot SCR_i \cdot SII_{i,M}^{CF} \tag{19}$$

where $SII_{i,M}^{CF}$ denotes the process- and material-specific impact intensity for milling at layer i, incorporating the layer-specific allowance coefficients ξ_i, ψ_i, χ_i:

$$\begin{aligned} SII_{i,M}^{CF} = \rho \cdot [(CI_{MatProd} + CI_{HF}) \cdot y_{HF} \cdot (1+\xi_i)(1+\psi_i)(1+\chi_i) + \\ CI_R \cdot (1+\xi_i)(1+\psi_i)\chi_i + CI_{SF} \cdot (1+\xi_i)\psi_i + CI_F \cdot \xi_i] \end{aligned} \tag{20}$$

2.2.3 Optimal processing route identification (Step D)

Once the layer-resolved impacts of the two processes are available, they are compared layer by layer: where the two profiles intersect, an intermediate transition between the processes may be advantageous. Because the workpiece for subtractive machining exists only up to the height at which deposition begins, a single transition is admissible, and only in the direction from subtractive to additive, since returning to milling from a solid block at the upper layers would not be feasible. Identifying the optimal switching point therefore consists in placing that single transition where the cumulative impact of the resulting route is lowest. This requires the cumulative impact to be expressed as a function of the position at which the transition is placed. For a hybrid route in which the transition occurs after layer k, the cumulative carbon footprint is obtained by combining the two layer-wise formulations:

$$CF_H(k) = \sum_{i=1}^{k} V_L \cdot SCR_i \cdot SII_{i,M}^{CF} + \sum_{i=k+1}^{n_L} V_L \cdot SCR_i \cdot SII_{i,W}^{CF} \tag{21}$$

where:

- $CF_H(k)$ is the carbon footprint of the hybrid route in which the transition occurs after layer k;
- k is the index of the last layer produced by milling.

At the two ends of the admissible range one of the two summations becomes empty. By this definition, $k=0$ corresponds to no layer being milled at all, so that the route is entirely additive (within the modeling framework adopted here): Eq. 21 reduces to Eq. 13 and $CF_H(0)$ coincides with CF_W. Conversely, for $k=n_L$ the transition would fall beyond the last layer and therefore does not take place, so that the route is entirely subtractive: Eq. 21 reduces to Eq. 19 and $CF_H(n_L)$ coincides with CF_M. The two single-process routes are therefore retrieved as limiting cases of the same formulation.

The optimal transition is the one that minimizes this quantity over the whole set of admissible positions, the argument of the minimum returning the layer at which the lowest value occurs rather than the value itself:

$$k^* = \operatorname{argmin}_{k \in \{0,\ldots,n_L\}} CF_H(k) \tag{22}$$

where k^* is the switching layer of the optimal hybrid route, selected among the n_L+1 admissible positions.

2.3 Case studies and data inventory

To demonstrate the applicability of the proposed modeling approach, three illustrative components (*Parts I*, *II*, and *III* in Figs. 4a-c) were specifically designed. These controlled benchmark geometries share similar features (i.e., concentric cylinders, arched ribs, and peripheral walls connecting the four corner cylinders within a parallelepiped volume) but differ in the spatial distribution of material, despite having identical part (V_p) and envelope (V_{env}) volumes. Consequently, they possess the same overall SCR but differ in their layer-resolved SCR_i profiles (Fig. 4d). Additionally, the mock-up of a real industrial component, a landing gear produced at the Welding and Additive Manufacturing Centre of Cranfield University (Cranfield, UK) and already referenced in literature, was included as a more realistic case study [28]. Initially, the manufacturing scenarios for all components (*Parts I*, *II*, *III*, and *landing gear*) were evaluated using AISI 308L Si steel. Subsequently, the analysis was conducted with Ti-6Al-4V titanium alloy, relevant for aerospace applications where metal wire deposition processes could be advantageous [29].

2.3.1 Material production and manufacturing

Eco-properties for both materials, together with the process-related input values used in Eqs. 12 and 18, are summarized in Table 2 and were primarily sourced from the ANSYS Granta Selector database, 2025 R1 release [8, 30]. Further

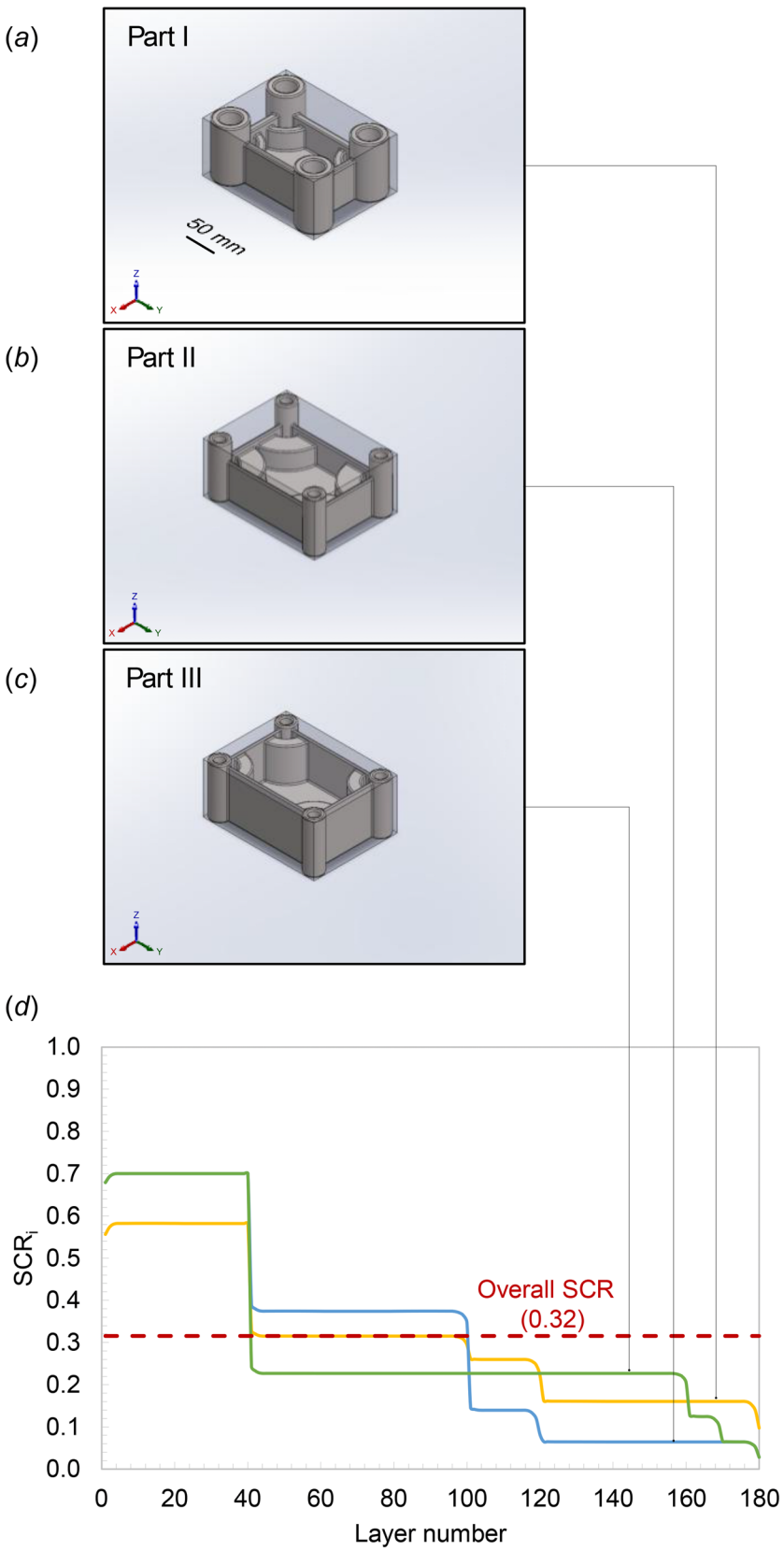


Fig. 4 **a**–**c** Parts I, II and III with identical overall SCR (0.32) and **d** different layer-by-layer SCR_i profiles due to varying material distribution within the envelope volume.

Table 2 Material eco-properties for AISI 308L Si and Ti-6Al-4V, including yield factors and carbon intensities associated with the different manufacturing stages considered [8, 30]. Note: in the present analysis, the carbon intensity associated with semi-finishing was assumed to be equal to that associated with roughing ($CI_{SF}=CI_R$)

Property description	Symbol (Unit)	AISI 308L Si	Ti-6Al-4V
Density	ρ (kg/mm^3)	$7.8–8.0 \cdot 10^{-6}$	$4.4–4.5 \cdot 10^{-6}$
Recycled content in the current supply (%)	R (%)	34%	49%
Yield factor, hot forming	y_{HF} (-)	1.00–1.11	
Yield factor, wire drawing	y_{WD} (-)	1.11–1.18	
Yield factor, WAAM	y_{WAAM} (-)	1.00–1.02	
CO_2 intensity, recycling	CI_{Rec} (kg/kg raw material)	1.73–1.91	11.7–12.8
CO_2 intensity, virgin grade production	CI_V (kg/kg raw material)	6.41–7.06	40.2–44.3
CO_2 intensity, typical grade production (RCA approach)	CI_{RCA} (kg/kg raw material)	4.82–5.31	26.2–28.9
CO_2 intensity, hot forming	CI_{HF} (kg/kg input material)	0.33–0.46	2.27–3.49
CO_2 intensity, wire drawing	CI_{WD} (kg/kg input material)	0.24–0.29	0.73–0.86
CO_2 intensity, WAAM	CI_{WAAM} (kg/kg deposited)	2.11–6.42	3.78–10.04
CO_2 intensity, roughing	CI_R (kg/kg removed)	1.05–1.17	1.69–2.08
CO_2 intensity, finishing	CI_F (kg/kg removed)	1.23–1.41	3.16–4.13

physical and mechanical properties of the two alloys are reported in Table 4 (Appendix). For parameters reported as ranges, the arithmetic mean was adopted for the average scenario, while the extremes defined the best- and worst-case scenarios. In fact, throughout the analysis, uncertainty is reported as [Min; Max] bounding intervals rather than as probabilistic confidence intervals. Each interval is delimited by two extreme scenarios: a best case (lower bound, Min), in which every input parameter is set to the value that minimizes the carbon footprint, and a worst case (upper bound, Max), in which every parameter is set to the value that maximizes it. Because the carbon-footprint model is monotonic with respect to the uncertain input parameters over the considered ranges, the two extreme combinations, in which all parameters are set to either their impact-minimizing or impact-maximizing values, bound the corresponding output. The resulting intervals are therefore conservative best/worst-case envelopes that, by construction, overstate the realistic dispersion, since the simultaneous occurrence of all parameters at the same extreme is improbable.

With regard to material production, the $CI_{MatProd}$ term introduced in Eqs. 7 and 15 for WAAM and milling, respectively, was calculated according to the Recycled Content Approach (RCA) [31], using the typical recycled content fraction (R) reported in Table 2 for each material. The values of R adopted are the recycled fraction in current supply reported by the same database, that is, the share of secondary material in the total worldwide production and supply of each material; they are assumed to be global averages. This typical-grade scenario represents the reference case for the whole analysis, combining the contribution of virgin material (CI_V) with that of recycled content and its associated recycling impact (CI_{Rec}). Finally, since material production dominates the total footprint and R is the free parameter of the RCA formulation, the robustness of the comparative assessment was examined through a sensitivity analysis on R. Starting from the virgin-grade case ($CI_{MatProd}=CI_V$), R was varied in 10% increments from 0 to 100% (corresponding to $CI_{MatProd}=CI_{Rec}$), so as to recalculate the effective carbon footprint under alternative supply mixes, including region-specific ones, and to assess the influence of R on the relative performance and on potential process switching between the considered manufacturing routes.

As for the impact of machining operations, the carbon intensities adopted for roughing and finishing are average estimates, reported by the database as including energy and heat together with the auxiliary materials used in the process. Therefore, cutting tools are not accounted for separately in the model. Since tool consumption scales with the volume of material removed, any residual omission would weigh most on the fully subtractive route, which removes the largest amount of material. The estimate reported for the milling-based scenario is therefore conservative: accounting for tool consumption explicitly would increase its carbon footprint and widen, rather than reduce, the margin by which the hybrid and additive routes outperform it. Moreover, although the proposed model parametrically defines machining allowances for roughing, semi-finishing and finishing, its practical use as a decision-support tool relies on readily accessible data, and the reference database provides comprehensive process information only for roughing and finishing operations. To address this limitation, the material volume allocated to semi-finishing is evaluated using the impact parameters of the roughing stage, consistent with the purpose of the model, which is to provide strategic guidance rather than high-fidelity simulation. Two considerations support this choice: the roughing stage is preponderant, as it accounts for the majority of the material removed; and, since the specific impact decreases as the material removal rate increases [19], the roughing and finishing values reported

in Table 2 bracket the semi-finishing one. The magnitude of the resulting error was quantified by repeating the calculation for *Part I* as a representative example, with the semi-finishing carbon intensity set to the finishing value, that is, the upper bound of that bracket: the total carbon footprint increases by at most 1.1% across the three scenarios and both materials. Moreover, this error affects the reported totals only: since the term $CI_{SF}\cdot(1+\xi_i)\psi_i$ appears identically in the specific impact intensities of the two routes (Eqs. 14 and 20), it cancels in their layer-wise difference, leaving the switching layer and the comparative ranking of the routes unaffected. Accordingly, the as-deposited WAAM geometry is defined in this model as the net-shape part combined with the finishing and semi-finishing allowances, the removal of the semi-finishing stock being evaluated with roughing impact parameters.

While milling-related impacts are reported in Table 2, WAAM process data refer to the experimental setup employed at the Welding and Additive Manufacturing Centre of Cranfield University, as detailed in [8]. Both shielding gas usage and electricity consumption were considered to estimate the associated CO_2-equivalent emissions. The CI_{gas} value adopted was $0.18\pm10\%$ kg CO_2 per kilogram of argon consumed during the active deposition phase [32]. Argon flow rates were 11.9 kg/h and 15.1 kg/h for steel and titanium, respectively, with corresponding deposition rates (DR) of 0.94 and 0.66 kg/h [8].

The CI_{WAAM} associated with electricity use was calculated using $eSEC_W$ values of 6.6 and 9.3 kWh per kg of deposited material for steel and titanium, respectively [8]. These values were multiplied by the carbon intensity of electricity consumption (CI_{elt}). The European Environment Agency provides the EU-27 GHG emission intensity factors for electricity generation for 2023, ranging from 0.008 kg CO_2 per kWh for Sweden to 0.594 kg CO_2 per kWh for Poland, representing the best- and worst-case scenarios, respectively (EU-27 average: 0.21 kg CO_2 per kWh) [33]. Consistently with the approach adopted for interval-valued inputs throughout this study, the arithmetic mean of the lower and upper bounds was used for the average scenario, while the two extremes defined the best- and worst-case scenarios. In this study, these production-based factors were adopted as a proxy for consumption-based intensity. To assess the implications of this assumption, a sensitivity analysis was carried out by adjusting the EEA factors to account for transmission and distribution (T&D) losses. A loss rate of 6% of the output power, as reported by the International Energy Agency [34] for the same year, was applied. This adjustment increased the total CI_{WAAM} by no more than 4% under the worst-case scenario. Given this marginal effect, the use of production-based emission factors as a proxy is considered a justified simplification for the scope of this analysis. The resulting CI_{WAAM} values were 4.3 [2.1–6.4] kg/kg for steel and 6.9 [3.8–10.0] kg/kg for titanium.

It should be noted that, for $eSEC_W$, only arc-on time (i.e., active deposition) was considered. The value adopted accounts for the deposition system and its auxiliary equipment, the chiller included, over the arc-on period, the energy consumption of the motion provision systems having been found negligible [8]. The same equipment continues to draw power during the interlayer intervals, but the corresponding energy is not included in the baseline, since their duration depends on process parameters, geometry, deposition path, heat dissipation, and cooling strategies, none of which are assumed to be known *a priori* when using the proposed decision-support tool. Since any additional consumption during dwell periods would elevate the final CI_{WAAM} value, a sensitivity analysis was performed on this parameter. The analysis acts on CI_{WAAM} as a whole, and not on the arc-on electric energy alone, and therefore subsumes every contribution that raises either the electricity or the shielding gas term: prolonged dwell, gas flow maintained even during idle periods, the energy drawn by auxiliary and standby loads, and differences in setup and energy mix between installations. For instance, applying the carbon intensities from this study to data from Catalano et al. [35] for a titanium component yields a CI_{WAAM} of 3.8–10.4 kg/kg, while data from Dias et al. [36] for steel deposition results in a CI_{WAAM} of 0.2–1.8 kg/kg. Given the uncertainty surrounding factors like part cooling and energy mixes in these external studies, a broad range was chosen to maximize the applicability of the model, with the CI_{WAAM} value varied from 1 to 20 kg/kg in the analysis.

2.3.2 CAD preparation and slicing

The envelope volume for the three controlled benchmark geometries was $200\times150\times90$ mm^3, while the landing gear component fit into a volume of $315\times340\times200$ mm^3. However, due to the symmetry of this part with respect to the XY plane, only half of the component was considered ($Z_{max}=100$ mm). To deposit the landing gear a foundational substrate was aligned with this plane. Using a component rotator, the application of the layers was alternated across the dual sides of the substrate, counterbalancing the stresses generated on one side by applying a layer to the opposing side [28]. Consequently, each analyzed half embeds one half of the substrate, and doubling the results consistently reconstructs the complete component, substrate included. In this study, SolidWorks 2024 was utilized for CAD modeling, while Autodesk Netfabb Premium 2024 was employed for the slicing process. Slicing was performed with a layer thickness of 0.5 mm, providing a good compromise between model accuracy and computational effort, considering the

medium-complexity geometries of the components. This value was intentionally selected to provide a geometric discretization finer than the minimum bead height. For example, in a study focused on the CMT deposition of 308L Si steel, the resulting bead heights (H) were observed to be in the range of 1.3 mm to 7.2 mm by combining Wire Feed Speed (WFS) values from 2 to 12 m/min and Travel Speed (TS) values from 0.1 to 0.9 m/min [37]. A convergence test on the chosen layer thickness was conducted by doubling and halving it and repeating the whole analysis. The test covered *Part I*, taken as representative of the three benchmark geometries, and the landing gear, in both steel and titanium: in every case the total carbon footprint varied by no more than 0.2% in absolute value and the switching height was unchanged. To ensure a consistent comparison, identical values were assigned to allowances to account for finishing operations for both materials adopted in the analysis (the choice of such values is discussed in detail in Sect. 2.3.2.1). This step was carried out in Netfabb using the 'Insert Offset' function. After adding each allowance (i.e., each offset), a.*csv* file was generated containing layer-specific data, including area and perimeter. The layer-wise geometric data were then processed to calculate the ξ, ψ and χ parameters, as well as the SCR_i values, for each layer. Finally, to quantify the carbon footprint, the equations introduced in Section 2.2.2 and Section 2.2.3 were implemented in MATLAB R2024a. This step produced impact values (i.e., equivalent carbon emissions) for each layer, depending on whether additive or subtractive processing was selected.

Machining allowances

Machining allowance refers to the excess material intentionally left on a near-net-shape component to ensure the required surface integrity and dimensional tolerances achieved in the final machining stage. Although there are suitable guidelines in casting and forging standards (e.g., ISO 8062–3), comparable guidelines for WAAM are still lacking [38]. As WAAM geometries are highly sensitive to process parameters, it is crucial to quantify variability in the as-deposited state rigorously in order to determine the size of the allowance and bridge the gap between the additive and subtractive stages [39, 40]. If the allowance is too small, residual asperities may not be eliminated; if it is too large, material consumption and machining time can increase [16]. The allowances must effectively counterbalance both the intrinsic deviations of the deposited surface (primarily layer-wise surface waviness accentuated along the build direction) and the additional errors introduced during fixturing and handling [38, 41]. Experiments on titanium thin walls have demonstrated that removing stock equivalent to the maximum peak-to-valley height (Sz) often leaves residual asperities. Therefore, at least $1.25 \times Sz$ should be removed [38, 42, 43]. Reported Sz values for steel and titanium WAAM parts range from approximately 0.5 mm to around 1.35 mm [44, 45]. The amplitude of waviness increases with heat input, influenced by deposition parameters such as wire feed speed, travel speed, and inter-pass temperature [43, 44, 46, 47]. For instance, some studies have shown that reduced heat input or enhanced inter-pass cooling can decrease waviness by up to 57% [41, 48]. Applying the $1.25 \times Sz$ factor to the upper bound of Sz (1.35 mm) for titanium yields an allowance of 1.69 mm. Similarly, Kokare et al. [16] recommend a uniform allowance of 2 mm across the entire surface to compensate for WAAM-induced waviness prior to final machining. Fuchs et al. [38] reported an Sz value of 1.92 mm for walls deposited at a WFS of 4–5 m/min, corresponding to an allowance value of 2.4 mm. A similar value can be estimated for steel. The machining allowance was conservatively dimensioned based on the average as-deposited thin-wall widths reported by Catalano et al. [37] for WFS = 3–5 m/min, where the width spans from 3.5 mm to 7.9 mm. Taking the worst-case scenario (where the WFS process parameters are unknown in this preliminary assessment), the semi-range equals 2.2 mm, which is taken as the baseline MA. To accommodate both materials, a single conservative allowance of 2.7 mm is adopted. This value can also compensate for inaccuracies induced by machine setup [38], given that the configuration of the hybrid process may not yet be known at the early design stage. Consequently, there is potential for inaccuracies in the setup if machining is performed on a different machine.

During the finishing process, 1.2 mm of allowance is considered, which is consistent with literature estimates of 1.0 mm and experimentally validated values of 1.25 mm. Frank et al. [49] demonstrated that this allowance yields high surface quality in electron-beam-melted titanium components. This choice aligns with the working assumption adopted in the present study that the material removed in the finishing step is equivalent to the machining allowance of a powder-bed-produced component, thereby enabling a like-for-like comparison. The remaining 1.5 mm is removed during semi-finishing.

3 Results and discussion

Figure 5 illustrates the results obtained from the analysis conducted on the three controlled benchmark geometries, assuming they were manufactured from steel. Figures 5a, b, and c show the average layer-by-layer ('LbL') impacts for *Parts I*, *II*, and *III*, respectively, with blue lines referring to the WAAM process ('Scenario W') and red lines referring to milling ('Scenario M'), considering the average values within the ranges provided for input data in Table 2. Solid lines indicate cradle-to-gate impacts considering, when

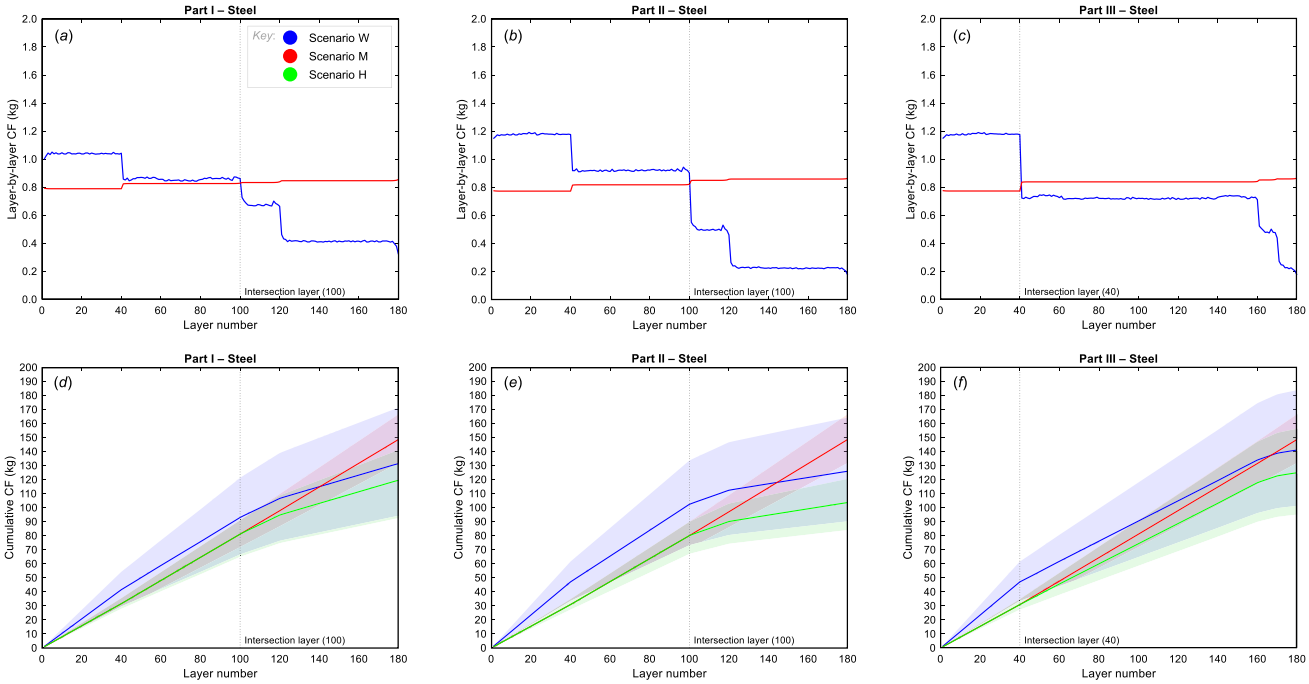


Fig. 5 Layer-by-layer **a**–**c** and cumulative **d**–**f** CF for *Parts I*, *II* and *III* in steel across WAAM (W), milling (M), and hybrid (H) scenarios; shaded areas indicate best- and worst-case ranges

assessing the impact of feedstock material production (and in particular during material production), the benefits deriving from the use of a certain percentage of recycled material (R, see Table 2) in the current supply [50]. LbL impacts for WAAM closely follow the SCR_i profiles (reported in Fig. 4d), as these impacts primarily depend on deposited material. Conversely, milling impacts arise from producing initially the entire layer and subsequently removing excess material to achieve the final geometry.

The intersections between the LbL curves represent the Z-levels at which the environmental impact of manufacturing a layer is equivalent for both processes, indicating an indifferent choice between the two. Beyond these points, milling consistently exhibits a higher environmental impact than WAAM, suggesting that a process switch from milling to WAAM would be advantageous from that layer onward.

Each iso-impact layer identifies a candidate switching location; the switching layer retained is the one that minimizes the cumulative hybrid footprint over all admissible positions. For the monotonic profiles of these components this minimum coincides with the single iso-impact layer, occurring at layer 100 for *Parts I* and *II* and at layer 40 for *Part III*. This behavior can be related to Fig. 4d, where layers 40 and 100 correspond to local step transitions in the SCR_i profiles of the three parts, occurring at different SCR_i values depending on the spatial distribution of material within the envelope. In particular, *Parts I* and *II* share an identical rib height at layer 100, where both profiles exhibit a comparable reduction in SCR_i, whereas *Part III* reaches a comparable condition already at layer 40, owing to its distinct combination of cylinder diameters and rib geometry.

In Figs. 5d–f, the cumulative values of the previously described curves are shown for each layer. The cumulative value at the final layer thus corresponds to the total CF associated with the production of the component, together with bands indicating the maximum and minimum values derived from the uncertainty range of input parameters used, standing for the best and worst-case scenarios. Compared to purely subtractive (milling, red curves), while employing purely additive processes (WAAM, blue curves), final values decreased by 11.9%, 15.6%, and 5.4% from Scenario M for *Parts I*, *II*, and *III*, respectively. Hybrid approaches combining milling and WAAM demonstrate more pronounced advantages, as illustrated by the green curves in Figs. 5d–f ('Scenario H'). For instance, in the case of *Part I* (Fig. 5d), the hybrid strategy involves milling a workpiece up to a height of 50 mm (based on an intersection layer at 100 and a slicing thickness of 0.5 mm), followed by WAAM to build the remaining features. As a result, the hybrid curve coincides with the milling curve up to the switching layer and thereafter evolves according to the WAAM layer-wise contributions, while retaining the cumulative impact accumulated during the initial milling stage, leading to overall impact reductions of 19.7% and 8.8% compared to milling and WAAM, respectively. The optimal switching layer varies depending on the specific geometry of each part (i.e.,

100, 100, and 40 for *Parts I*, *II*, and *III*, respectively). As a result, cumulative impact calculations for hybrid manufacturing begin summing the additive contributions from different Z-levels. This finding indicates that components with identical envelope volumes and overall SCR can still exhibit different environmental performances when produced using hybrid approaches within the modeled configurations.

In Fig. 6 the results from the two sensitivity analyses are reported. Figure 6a illustrates the total impact values for each *R* percentage (for *Part I*). When exclusively using virgin source material, comparing the two approaches, the WAAM-based process is preferable (153.7 kg compared to 188.6 kg). This preference remains valid until *R* reaches 69%, beyond which machining becomes more advantageous. For the analyzed case ($R=34\%$), WAAM is marginally more advantageous than machining (as shown in Fig. 6a). As for CI_{WAAM} (Fig. 6b), at lower values, WAAM is clearly the least carbon-intensive process, and this advantage persists up to approximately $CI_{WAAM}=5.8$ kg/kg, beyond which machining becomes more favorable for the geometry considered. It is worth noting that this threshold falls within the range calculated considering best- and worst-case electricity generation intensities in EU-27 energy mixes (resulting in $CI_{WAAM}=2.1$ to 6.4 kg/kg), indicating that the optimal processing route for steel parts could vary slightly depending on the location of production.

In the analyzed cases, the hybrid approach effectively combines the strengths of both processes, tending to yield lower total impacts than either individual route. Figure 6b also shows the corresponding switching layer, defined as the Z-level at which switching between processes is recommended. At $CI_{WAAM}=1$ kg/kg, Scenario W and Scenario H coincide (i.e., no process switch is required, and the part would be theoretically manufactured entirely via WAAM). For higher CI_{WAAM} values, the intersection layer shifts progressively, indicating that only the material to be deposited from that layer onward remains advantageous to be deposited via WAAM. For CI_{WAAM} values in the 17–20 kg/kg range, the recommended intersection layers are 177–179, therefore 1.5–0.5 mm before the completion of the part considering the 0.5-mm slicing thickness. In such a scenario, a process switch would not be practically advantageous. The environmental savings would be negligible, and the logistical complexity of switching processes for such a small feature would likely outweigh any marginal benefit.

This gives rise to a further reflection on the practicality of a process switch. The decision to move from a subtractive to an additive process is a techno-economic consideration that must account for a feasibility threshold. If the model indicates that the switch is only beneficial for a minimal portion of the part, the logistical overhead could outweigh the environmental savings, especially in a decentralized production model that would require shipping a semi-finished component. However, this barrier is progressively being eliminated using integrated hybrid manufacturing systems, which combine additive and subtractive capabilities within a single machine. In such a setup, many of the logistical challenges are reduced: the need for transportation is eliminated, the component remains in the same fixture, which solves any issue related to re-positioning and the setting of machine zeros, and the entire workflow is streamlined to minimize lead times. In this context, even a switch for a relatively small portion of the part may become not only feasible, but also strategically advantageous, although its overall techno-economic convenience would still require case-specific assessment. Therefore, while the proposed framework provides a quantitative tool to identify the environmental potential, the ultimate decision on the practicality

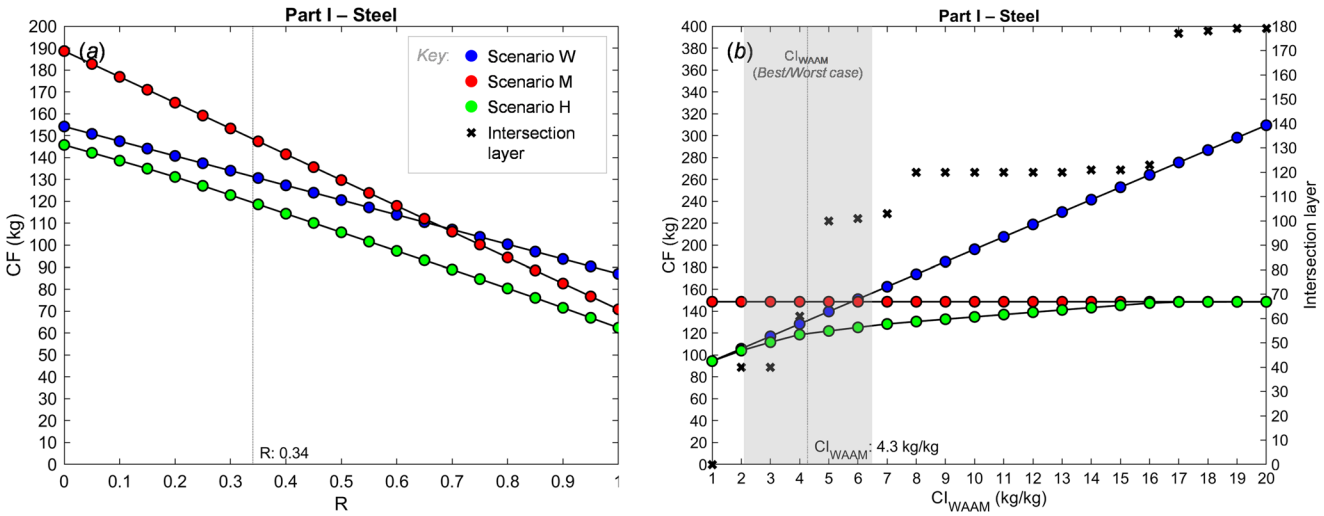


Fig. 6 Sensitivity analysis for *Part I* (in steel): **a** effect of recycled content in the current supply (*R*), **b** effect of CI_{WAAM} on total CF for Scenario M (milling), W (WAAM), and H (hybrid); crosses indicate the layer at which the layer-by-layer curves of M and W intersect

of the switch should also be evaluated based on the specific technological capabilities available.

To further support the claim that identical features can result in different environmental impacts depending on how they are spatially distributed within the envelope volume, *Part I* was compared to a modified version of it. In this variant, the envelope volume was increased along the X-direction, from 200 to 400 mm, while keeping the geometric features unchanged (namely the cylinders and arched ribs). Only the external walls were extended to span the entire parallelepiped (Fig. 7). With the geometric features kept unchanged, altering one of the envelope dimensions changes the corresponding SCR_i values (since SCR_i depends on the envelope volume) and, consequently, the amount of material to be removed to obtain the same features. This effect is confirmed by the *i*-th impact values shown in Figs. 7b and c, where the layers corresponding to those feature sections identified in Fig. 7a are highlighted. While the *i*-th impacts associated with WAAM remain unchanged, those related to milling differ by 0.85 kg per layer: milling CF per layer doubles between *Part I* (0.84 kg/layer) and its variant with an increased X dimension (1.69 kg/layer), due to the greater amount of material that must be removed as a result of the increased XY area of the envelope.

Using the same model but employing the eco-properties of the titanium alloy Ti-6Al-4V allowed for a comparative analysis to evaluate how results vary across different material choices for identical geometries. For brevity, Fig. 8 presents results only for *Parts I* and *II* (manufactured in titanium alloy).

When examining the LbL impacts, Fig. 8a shows that WAAM consistently outperforms milling for *Part I*, with no iso-emission point being observed. As a result, no switch between processes is suggested. Consequently, the average cumulative CF curve for the hybrid route exactly overlaps with that of the WAAM-based process throughout all layers of the component. Since the analysis is repeated independently for the average, best-case, and worst-case input combinations, the corresponding optimal switching layer k^* may differ among these scenarios. This indicates that input-data uncertainty can affect not only the magnitude of the resulting CF, but also the recommended process transition (e.g., in Fig. 8c). In this case, $k^*=40$ only for the worst case leads to a marginal difference in the final results, where the cumulative CF is 348.8 kg for Scenario W (Max) and 342.6 kg for Scenario H (Max).

The situation differs for *Part II*, where the initial portion is better manufactured through a milling-based approach, followed by a transition to WAAM at layer 40. In this case, total CF decreases from 426.3 kg (Scenario M) to 276.2 kg (Scenario W), and further to 264.6 kg (Scenario H).

This confirms that, from a methodological standpoint, despite only an 8.1%-difference between *Parts I* and *II* considering the minimum total CF values, the two components require different processing routes, even though their overall SCR values are the same. Moreover, for the milling-based approach, the total CF for both *Parts I* and *II* is nearly identical (≈ 426 kg), an expected outcome given their shared overall SCR and identical envelope volume V_{env}. For the WAAM-based approach, however, the same overall SCR does not yield an equivalent CF, resulting in a slight discrepancy between the two parts (288 kg vs. 276 kg). This highlights that overall SCR alone is an insufficient predictor for WAAM; the outcome is instead driven by the internal, layer-wise distribution of material (i.e., the SCR_i profile), which alters the deposited allowance volume. Despite the CF difference being limited in this case to 4.1%, this finding underscores the benefit of a layer-resolved analysis for such processes.

Finally, the symmetrical landing gear mock-up was analyzed, focusing on one half of the component (Fig. 9a); therefore, the reported CF values should be doubled to account for the impact of the full component. For the titanium alloy, the layer-by-layer impacts (Fig. 9b) show that the WAAM-based route is disadvantageous only for the base region, up to layer 24. For steel, this intersection layer shifts to 30. Beyond these respective thresholds, WAAM consistently becomes the more advantageous option. Figures 9c and 9 d compare the cumulative impact curves for both materials, highlighting the ranges between best- and worst-case scenarios. For both steel (Fig. 9c) and titanium (Fig. 9d), Scenario H consistently represents the most favorable option. Among the single-process routes, WAAM consistently outperforms milling.

The same sensitivity analyses conducted for the three controlled benchmark geometries (*Parts I*, *II* and *III*) were also performed for the landing gear considering both materials. These analyses considered the recycled material content in the current supply, *R* (Figs. 9e and f), as well as CI_{WAAM} (Figs. 9g and h). For both steel and titanium, for any value of *R*, milling remains consistently more carbon-intensive than WAAM among the single-process routes. For CI_{WAAM}, increasing its value from 1 to 20 kg/kg results in a substantial rise in total CF for steel, from 224.2 to 741.1 kg, corresponding to an increase of 230.6%. For titanium, the effect is more limited, with total CF increasing from 603.9 to 893.5 kg, or approximately 48.0%. This variation causes only a slight upward shift in the recommended switching layer between the two processes. Moreover, for steel, from $CI_{WAAM}=14.0$ kg/kg onwards, the milling-based route becomes more advantageous than the WAAM-based route, although Scenario H remains the lowest-impact option. For titanium, however, no inversion in the relative

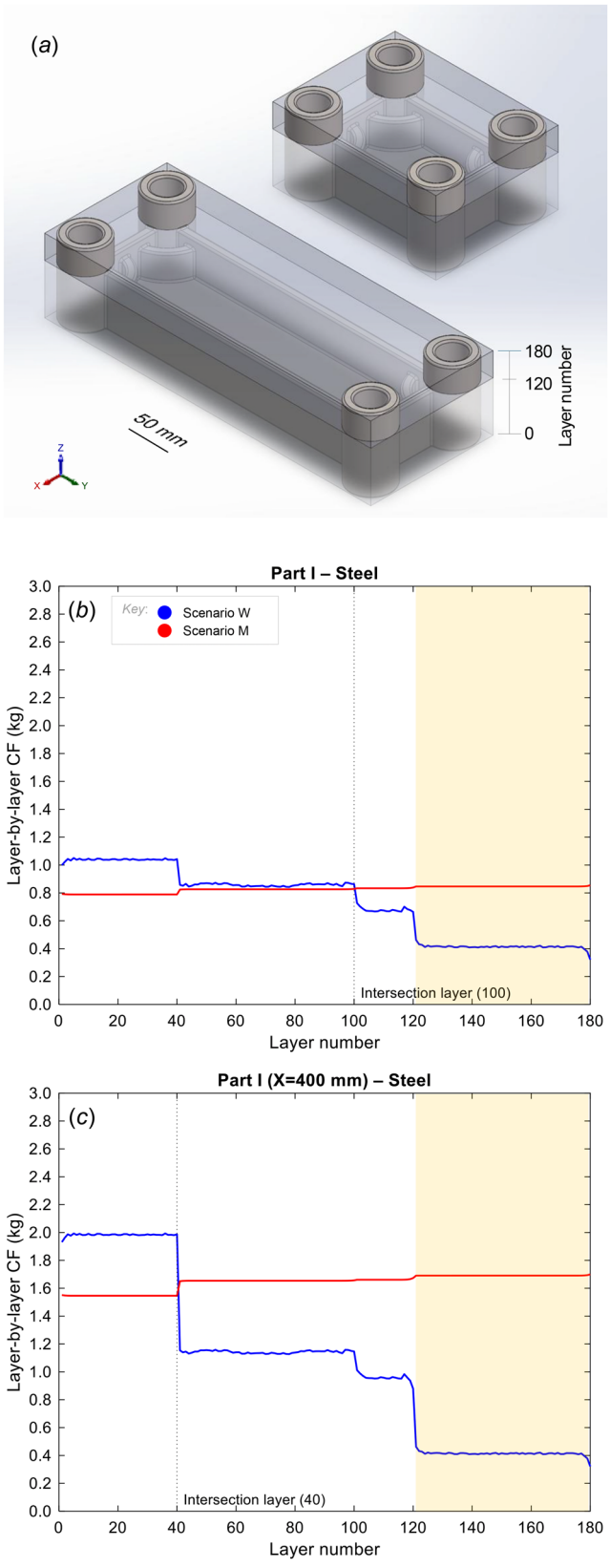


Fig. 7 **a** Highlighted portions of identical features in *Part I* and its extended-envelope variant (in X-direction); **b**–**c** corresponding layer-by-layer CF with shaded regions referring to those portions (increased impact for Scenario M; Scenario W unaffected).

environmental performance of the two processing routes occurs over the investigated CI_{WAAM} range: WAAM remains preferable to milling, while Scenario H remains the lowest-impact option.

3.1 Summary of the results

The results of the analyses are summarized in Table 3, which compares the carbon footprint of the three processing routes. Across the modeled case studies, the proposed framework establishes the size of the carbon footprint reduction and the optimal position of the switching layer (k^*). Because k^* is determined as the position of the minimum cumulative impact across all possible layers, a set that intrinsically includes both the purely subtractive and purely additive extremes, Scenario H yields, by definition, the lowest-impact configuration. The case studies quantify the magnitude of this reduction, which is particularly marked for the titanium landing gear, where a decrease in impact of up to 61.2% is observed compared to Scenario M, and reaches 17.5% compared to Scenario W for the steel *Part II*. At the same time, the results illustrate that a mixed subtractive-additive approach is not universally necessary to minimize emissions. For example, for *Part I* in titanium, $k^*=0$ and Scenario H coincides entirely with Scenario W. This highlights that the framework correctly defaults to a single-process route when a mixed strategy offers no additional environmental benefit, reporting a true hybrid advantage only where it quantitatively exists.

Figure 10 presents the same results graphically, with the [Min; Max] intervals shown as error bars. The overview makes two of the effects discussed above clearly visible: the coincidence of Scenarios W and H for *Part I* in titanium, where no process switch is required, and the near equality of the Scenario M values across *Parts I*, *II* and *III*, which share the same overall SCR despite their different material distributions.

In the components analyzed, the SCR_i profiles are monotonic and descending (Fig. 4d), and wherever a switch is beneficial the LbL impacts for Scenario M and W intersect only once (Figs. 5a-c, 8b, and 9b), so that the switching layer identified by Eq. 22 coincides with that intersection. A second intersection could occur, for example, if the part cross-sectional area or the layer-specific allowance ratios increased again along the build direction. More generally, any part with undercuts or features with significant overhangs may require support structures, which would therefore need to be considered in the model as material to be removed. Overall, this modeling method is particularly suited to geometries of medium complexity typical of "demoldable" components, such as those produced by molding or casting followed by machining. If these processes were considered to produce

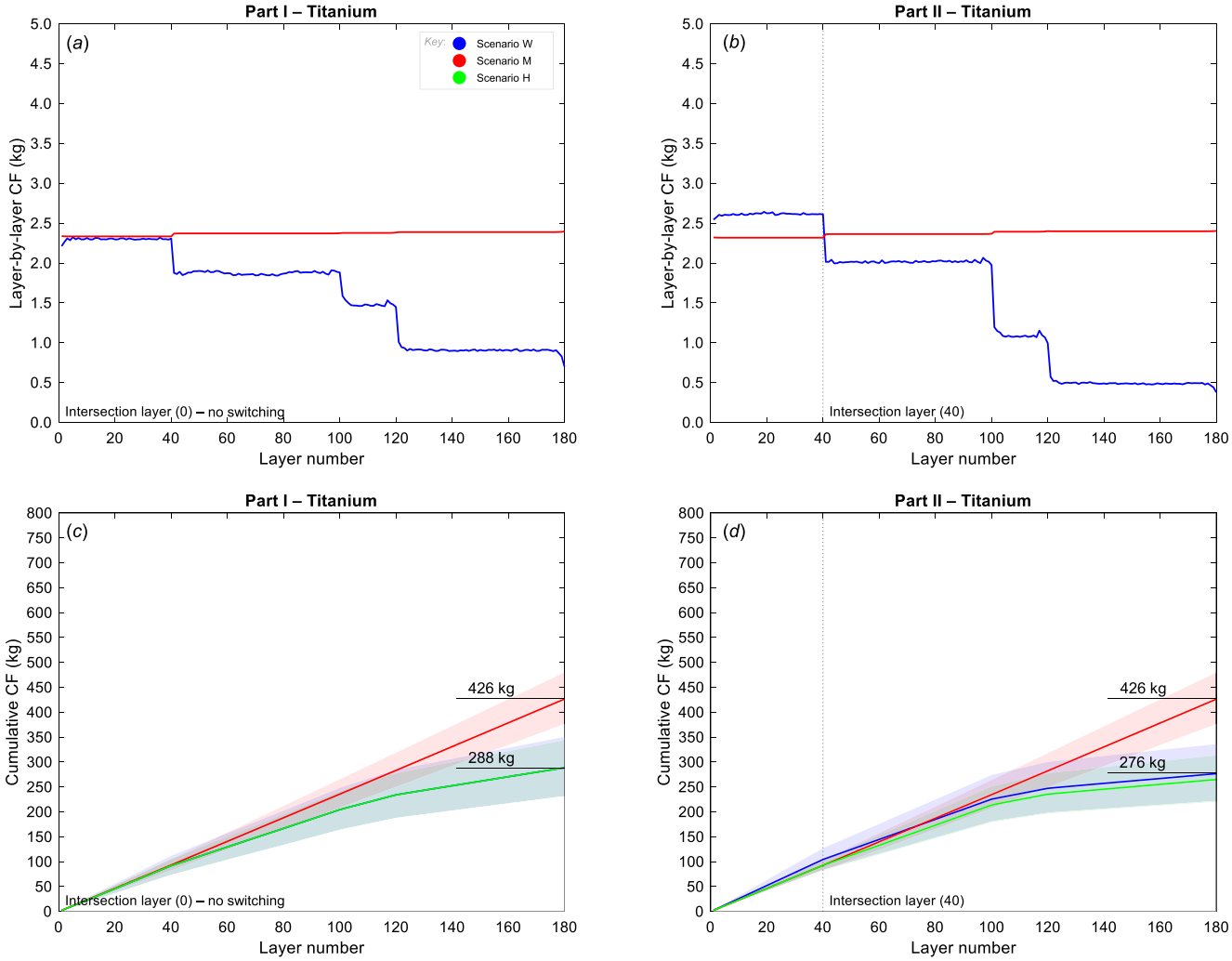


Fig. 8 Layer-by-layer **a**–**b** and cumulative **c**–**d** CF for Parts I and II manufactured in titanium alloy, comparing Scenarios W (WAAM), M (milling), and H (hybrid)

the near-net-shaped part, however, it would also be necessary to include the impact of mold creation and evaluate batch size. This study, on the other hand, aims to leverage the advantages of additive manufacturing in contexts where no special tooling is required, such as prototypes, customized components, or small batches of on-demand parts.

4 Conclusions

Given the substantial contribution of manufacturing to global GHG emissions, selecting the most appropriate process represents a relevant lever for reducing environmental impacts. This study introduced a modeling framework for the environmental assessment of hybrid manufacturing routes combining WAAM-based additive and subtractive processes. The proposed framework provides a systematic decision-support tool applicable at the early design stage for manufacturing route selection. By adopting a layer-resolved analysis based on the Solid-to-Cavity Ratio (SCR_i), the framework enables the identification of optimal switching points between milling and WAAM, with the goal of minimizing environmental impacts and product carbon footprint. The numerical results presented in this work are primarily intended as representative case studies used to demonstrate the proposed methodology, rather than as statistically generalizable evidence across the full spectrum of possible geometries and process configurations.

Across the case studies considered in this work, including three controlled benchmark geometries (*Parts I*, *II*, and *III*) and a representative landing gear component evaluated for both steel and titanium alloys, the hybrid approach generally resulted in lower total impacts compared to the individual manufacturing strategies. An exception was observed for *Part I* produced in titanium, for which the purely WAAM route yielded the lowest modeled CF within

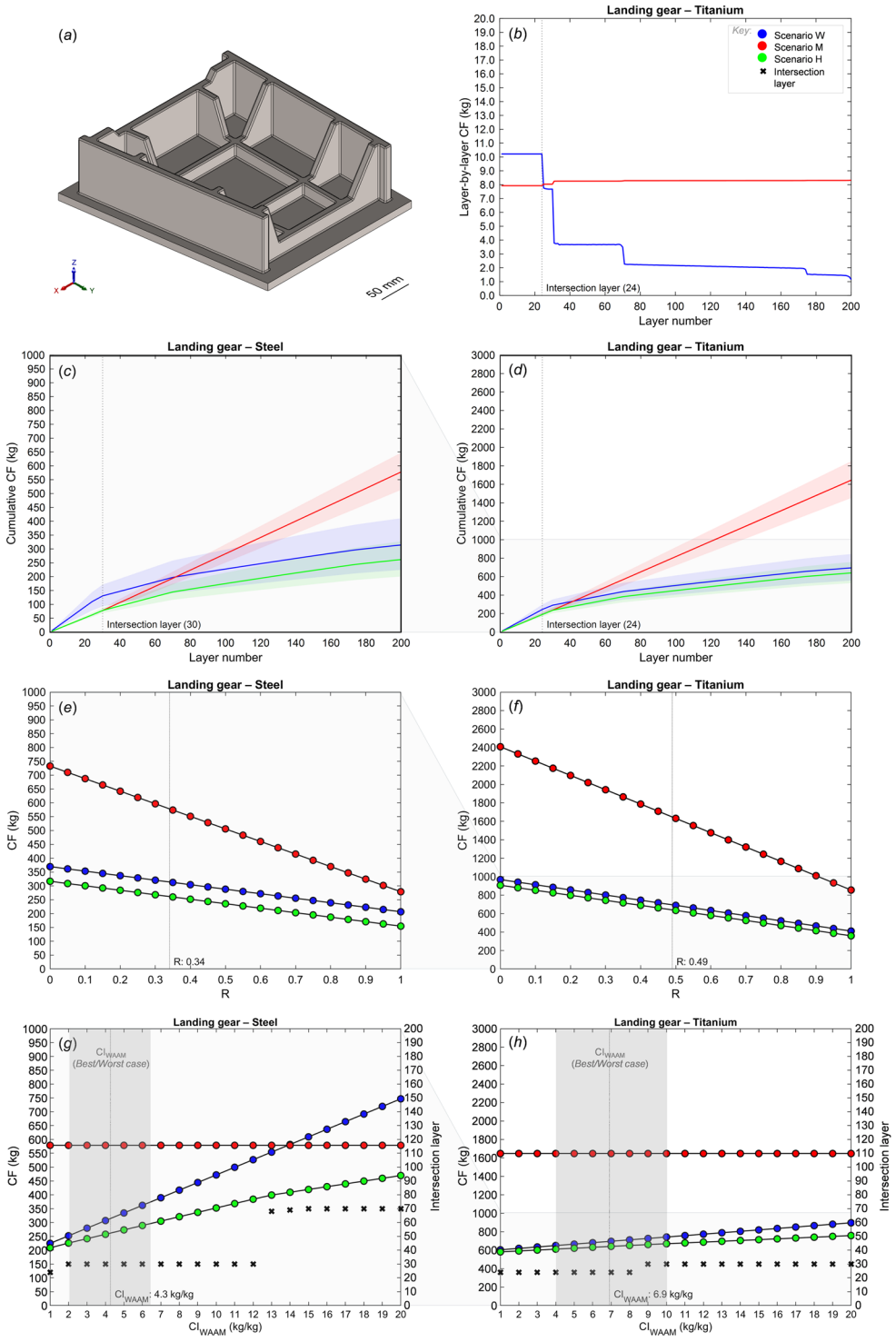


Fig. 9 Landing gear case study: **a** CAD of the component, and **b** layer-by-layer CF for titanium. Material-based comparison under Scenarios M (milling), W (WAAM), and H (hybrid): **c**-**d** cumulative CF; sensitivity to **e**–**f** recycled content in the current supply (*R*) and (*g*-*h*) CI_{WAAM}; crosses indicate the layer at which the layer-by-layer curves of M and W intersect. Note: results correspond to one half of the component

the investigated scenarios. For example, in the case of *Part I* produced in steel, hybrid manufacturing reduced total CF by 19.7% compared to milling and by 8.8% compared to WAAM, while for the titanium landing gear, these reductions reached 61.2% and 7.9%, respectively. The analysis indicates that identical overall SCR values may not necessarily translate into identical environmental outcomes, as the internal distribution of material within the envelope can influence results depending on the processing route. While the milling-based scenario yielded nearly identical impacts for *Parts I* and *II* (~426 kg), the WAAM-based route showed a slight difference (288 kg versus 276 kg) due to variations in layer-resolved SCR_i. This suggests that accounting for spatial material distribution is important when evaluating

Table 3 Summary of the total CF, expressed in kg $CO_{2\ eq}$, for each component and material analyzed. The table compares the average values (Avg) and best- and worst-case intervals [Min; Max] for the milling-based (M), WAAM-based (W), and hybrid (H) manufacturing scenarios (the last two columns quantify the percentage reduction in impact of the hybrid scenario compared to the subtractive and additive scenarios)

		CF (kg)							
Component	Material	Scenario M		Scenario W		Scenario H			
		Avg	[Min; Max]	Avg	[Min; Max]	Avg	[Min; Max]	↓% vs M	↓% vs W
Part I	Steel	148.6	[131.9; 166.6]	130.9	[94.2; 169.7]	119.3	[92.5; 140.5]	19.7%	8.8%
	Titanium	426.5	[376.4; 479.8]	288.0	[231.5; 348.8]	288.0	[231.5; 342.6]	32.5%	0.0%
Part II	Steel	148.6	[131.8; 166.5]	125.4	[90.2; 162.6]	103.5	[84.0; 120.1]	30.4%	17.5%
	Titanium	426.3	[376.3; 479.6]	276.2	[222.0; 334.6]	264.6	[220.0; 312.5]	37.9%	4.2%
Part III	Steel	148.6	[131.9; 166.6]	140.5	[101.3; 182.1]	124.5	[95.1; 155.5]	16.2%	11.4%
	Titanium	426.6	[376.5; 479.9]	308.5	[248.1; 373.7]	297.0	[246.1; 351.6]	30.4%	3.8%
Landing gear (half)	Steel	578.6	[513.7; 648.2]	313.1	[224.4; 406.9]	261.0	[200.5; 325.0]	54.9%	16.6%
	Titanium	1647.2	[1453.9; 1852.8]	694.0	[557.6; 841.1]	639.5	[528.9; 756.6]	61.2%	7.9%

Landing gear values refer to one half of the symmetric component (Z_{max} = 100 mm); multiply by two to obtain the impact of the full part. Relative reductions are unaffected

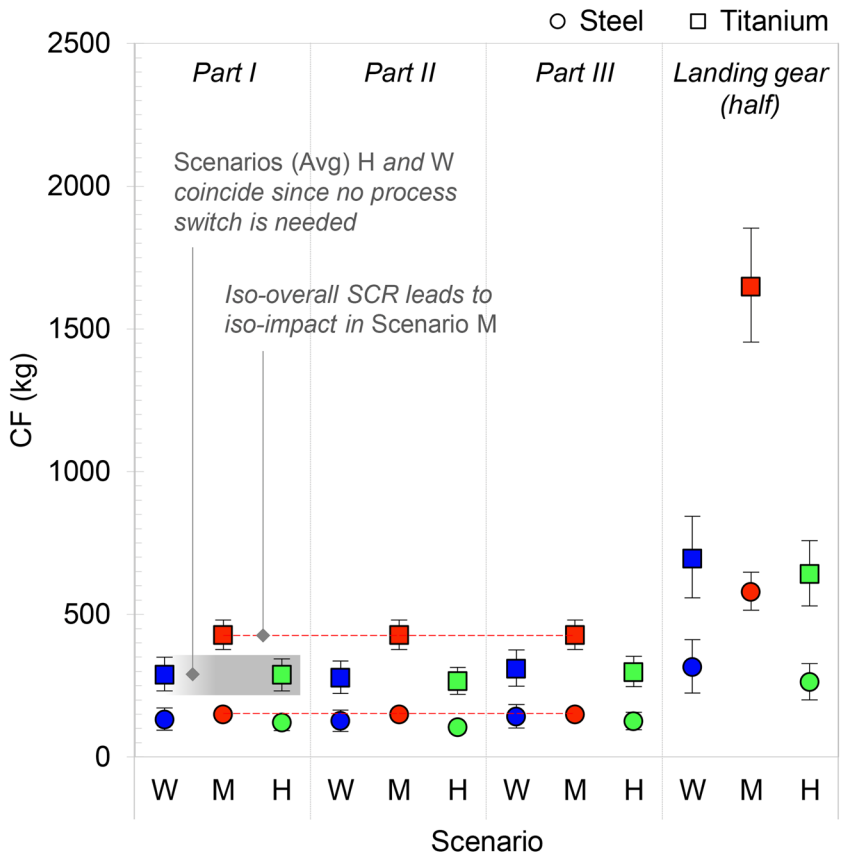


Fig. 10 Total carbon footprint for all case studies, grouped by component and manufacturing scenario. Error bars indicate [Min; Max] bounds. Note: Landing gear values refer to one half of the symmetric component

WAAM-based or hybrid processes, as global indicators such as overall SCR may not fully capture layer-wise geometric effects. Moreover, identical geometric features may result in different environmental impacts when embedded within envelopes of different sizes. Increasing the X-dimension of the envelope from 200 to 400 mm, while keeping the internal features of *Part I* unchanged, doubled the milling impacts, from 0.84 kg to 1.69 kg per layer, due to the greater material volume to be removed. In contrast, the WAAM impact for these layers remained constant, as the deposited volume is independent of the envelope size. This finding highlights the influence of spatial material distribution within the selected reference envelope.

Sensitivity analyses showed that the recycled content in the material supply can influence process selection for steel parts, potentially reversing the ranking between milling and WAAM. In contrast, for the titanium landing gear, WAAM remained the most favorable option within the investigated recycled-content range. An additional sensitivity analysis on the carbon intensity of the WAAM process (CI_{WAAM})

was conducted to assess the robustness of the findings with respect to contributions not explicitly modeled in CI_{WAAM}, namely prolonged dwell, shielding gas maintained during idle periods, auxiliary and standby loads, and differences in setup and energy mix between installations. Increasing CI_{WAAM} shifted the optimal switching point, with a more pronounced effect for steel than for titanium. For steel, higher CI_{WAAM} values led to a reversal in the ranking between WAAM and milling among the single-process routes at specific thresholds (e.g., 5.8 kg/kg for *Part I* and 14 kg/kg for the landing gear). For the titanium landing gear, no change in preference was observed within the investigated CI_{WAAM} range. These results suggest that these unmodeled contributions may be more influential for steel components when CI_{WAAM} approaches the identified threshold values, particularly within ranges associated with EU-27 electricity generation intensities.

The proposed SCR_i-based decision-support framework may be applicable in sectors where both additive and subtractive capabilities are relevant, such as aerospace, energy, tooling and heavy equipment industries. Integrating it early in design can help process planners avoid over-specifying AM for massive geometries or over-relying on SM for low-utilization features. Based on the analyzed configurations, recurring patterns were observed: when SCR_i remains consistently high along the build height, subtractive manufacturing tends to exhibit lower impacts; when consistently low, additive manufacturing tends to be more advantageous; and when SCR_i varies significantly along the build direction, hybrid strategies are more likely to reduce total impacts, with the process transition placed at the layer that minimizes the cumulative footprint. Local energy mixes and process conditions may shift this switching point or justify retaining subtractive operations for initial layers. Overall, the presented framework is implementable in industrial practice and is intended to provide fast, geometry-aware guidance for case-specific route selection, complementing rather than replacing detailed engineering analysis.

These findings should be interpreted in light of some limitations and within the specific modeling scope adopted in this study. The framework relies on a layer-resolved analysis with constant layer thickness and assumes a single transition between the two processes, in the direction from subtractive to additive, consistent with the availability of workpiece material only up to the switching height. The machining impact assessment is based on available database information for roughing and finishing operations, with semi-finishing impacts approximated using roughing parameters to preserve the rapid decision-support objective of the model. Practical WAAM manufacturing from scratch inherently requires a conventionally produced substrate; within the present framework, such configurations are represented as hybrid routes, with the switching point corresponding to the substrate thickness. Furthermore, only arc-on specific energy consumption was explicitly modeled for WAAM, while other contributions to CI_{WAAM}, including dwell, idle shielding-gas flow, auxiliary and standby loads, and setup and energy-mix differences, were addressed through sensitivity analysis. Accordingly, the methodology is primarily intended for early-stage comparative evaluation of medium-complexity geometries, rather than detailed process-level simulation or optimization, and should not be interpreted as directly generalizable across all component families, materials, or manufacturing contexts. Future work should integrate additional performance indicators such as processing time, production cost, and broader environmental categories, enabling a comprehensive multi-criteria decision analysis, and extend the application of the framework to a broader portfolio of real industrial parts and process data in order to more thoroughly assess the external validity and practical transferability of the insights obtained in this study.

Appendix

Table 4 Physical and mechanical properties of AISI 308L Si and Ti-6Al-4V, as reported by the ANSYS Granta Selector database [30]

Property (unit)	AISI 308L Si	Ti-6Al-4V
Young's modulus (GPa)	189–197	110–119
Yield strength (MPa)	187–227	786–910
Tensile strength (MPa)	500–600	860–980
Elongation (% strain)	50–70	10–14
Specific strength (kN·m/kg)	23.6–28.7	177–206
Hardness, Vickers (HV)	160–200	337–373
Weldability	Excellent	Good

Author contributions **Angioletta R. Catalano:** Conceptualization; Methodology; Software; Validation; Formal analysis; Investigation; Data curation; Writing – original draft; Writing – review & editing; Visualization. **Emanuele Pagone:** Methodology; Validation; Writing – review & editing; **Eloïse Eimer:** Methodology; Validation; Writing – review & editing; Investigation; **Paolo C. Priarone:** Resources; Supervision; Writing – review & editing. **Luca Settineri:** Supervision.

Funding Open access funding provided by Politecnico di Torino within the CRUI-CARE Agreement.

Data availability The manuscript has no associated data or supplementary information. Data will be made available upon request.

Declarations

Conflict of interest On behalf of all authors, the corresponding author states that there is no conflict of interest.

Open Access This article is licensed under a Creative Commons Attribution 4.0 International License, which permits use, sharing, adaptation, distribution and reproduction in any medium or format, as long as you give appropriate credit to the original author(s) and the source, provide a link to the Creative Commons licence, and indicate if changes were made. The images or other third party material in this article are included in the article's Creative Commons licence, unless indicated otherwise in a credit line to the material. If material is not included in the article's Creative Commons licence and your intended use is not permitted by statutory regulation or exceeds the permitted use, you will need to obtain permission directly from the copyright holder. To view a copy of this licence, visit http://creativecommons.org/licenses/by/4.0/.

References

1. Bashmakov IA, Nilsson LJ, Acquaye A, et al (2022) Industry. In: Shukla PR, Skea J, Slade R, et al (eds) Climate Change 2022: Mitigation of Climate Change. Contribution of Working Group III to the Sixth Assessment Report of the Intergovernmental Panel on Climate Change. Cambridge University Press, Cambridge, UK and New York, NY, USA, pp 1161–1244. https://doi.org/10.1017/9781009157926.013
2. International Energy Agency (IEA) (2023) Net Zero Roadmap: A Global Pathway to Keep the 1.5 °C Goal in Reach – 2023 Update. IEA, Paris. https://www.iea.org/reports/net-zero-roadmap-a-global-pathway-to-keep-the-15-c-goal-in-reach. Accessed 15 July 2026
3. Liu W, Deng K, Wei H et al (2021) A decision-making model for comparing the energy demand of additive-subtractive hybrid manufacturing and conventional subtractive manufacturing based on life cycle method. J Clean Prod 311:127795. https://doi.org/10.1016/j.jclepro.2021.127795
4. Şükrü Adin M (2024) A study on additive manufacturing processes, standards and mechanical properties. Post-processing of parts and components fabricated by fused deposition modeling, 1st ed. CRC Press, Boca Raton, pp 213–231. https://doi.org/10.1201/9781032665351-15
5. Gradl P, Tinker DC, Park A et al (2022) Robust metal additive manufacturing process selection and development for aerospace components. J Mater Eng Perform 31:6013–6044. https://doi.org/10.1007/s11665-022-06850-0
6. Wortmann N, Jürgenhake C, Seidenberg T et al (2019) Methodical approach for process selection in additive manufacturing. Proc Des Soc Int Conf Eng Des 1:779–788. https://doi.org/10.1017/dsi.2019.82
7. Schuhmann D, Rupp M, Merkel M, Harrison DK (2022) Additive vs. conventional manufacturing of metal components: selection of the manufacturing process using the AHP method. Processes 10:1617. https://doi.org/10.3390/pr10081617
8. Priarone PC, Pagone E, Martina F et al (2020) Multi-criteria environmental and economic impact assessment of wire arc additive manufacturing. CIRP Ann 69:37–40. https://doi.org/10.1016/j.cirp.2020.04.010
9. Wang Z, Yan X, Bjorni J et al (2024) Manufacturing process selection based on similarity search: incorporating non-shape information in shape descriptor comparison. J Intell Manuf 36:2509–2536. https://doi.org/10.1007/s10845-024-02368-5
10. Zhang W, Zhang P, Zhang J (2020) A decision-support model to select forming principle of part for sustainable manufacturing. 2020 asia-pacific international symposium on advanced reliability and maintenance modeling (APARM) 1–5https://doi.org/10.1109/APARM49247.2020.9209451
11. Paris H, Mokhtarian H, Coatanéa E et al (2016) Comparative environmental impacts of additive and subtractive manufacturing technologies. CIRP Ann 65:29–32. https://doi.org/10.1016/j.cirp.2016.04.036
12. Priarone P, Ingarao G, di Lorenzo R, Settineri L (2017) Influence of material-related aspects of additive and subtractive Ti-6Al-4V manufacturing on energy demand and carbon dioxide emissions. J Ind Ecol 21:S191–S202. https://doi.org/10.1111/jiec.12523
13. Ingarao G, Priarone PC (2020) A comparative assessment of energy demand and life cycle costs for additive- and subtractive-based manufacturing approaches. J Manuf Process 56:1219–1229. https://doi.org/10.1016/j.jmapro.2020.06.009
14. Siva Rama Krishna L, Srikanth PJ (2021) Evaluation of environmental impact of additive and subtractive manufacturing processes for sustainable manufacturing. Mater Today Proc 45:3054–3060. https://doi.org/10.1016/j.matpr.2020.12.060
15. Reis RC, Kokare S, Oliveira JP et al (2023) Life cycle assessment of metal products: a comparison between wire arc additive manufacturing and CNC milling. Adv Industrial Manufacturing Eng 6:100117. https://doi.org/10.1016/j.aime.2023.100117
16. Kokare S, Oliveira JP, Godina R (2023) A LCA and LCC analysis of pure subtractive manufacturing, wire arc additive manufacturing, and selective laser melting approaches. J Manuf Process 101:67–85. https://doi.org/10.1016/j.jmapro.2023.05.102
17. Liu Z, Islam F, Era IZ, Grandhi M (2023) LCA-based environmental sustainability assessment of hybrid additive manufacturing of a turbine blade. Green Manufacturing Open 2:1. https://doi.org/10.20517/gmo.2022.08
18. Liu X, Zhao G, Zhang H et al (2022) The carbon emission comparison between hybrid manufacturing and conventional processes based on bionic computing of industrial metabolism. Energy Rep 8:420–431. https://doi.org/10.1016/j.egyr.2022.10.331
19. Campatelli G, Montevecchi F, Venturini G et al (2020) Integrated WAAM-subtractive versus pure subtractive manufacturing approaches: an energy efficiency comparison. Int J of Precis Eng Manuf-Green Tech 7:1–11. https://doi.org/10.1007/s40684-019-00071-y
20. Le VT, Paris H (2018) A life cycle assessment-based approach for evaluating the influence of total build height and batch size on the environmental performance of electron beam melting. Int J Adv Manuf Technol 98:275–288. https://doi.org/10.1007/s00170-018-2264-7
21. Lyons R, Newell A, Ghadimi P, Papakostas N (2021) Environmental impacts of conventional and additive manufacturing for the production of Ti-6Al-4V knee implant: a life cycle approach. Int J Adv Manuf Technol 112:787–801. https://doi.org/10.1007/s00170-020-06367-7
22. Priarone P, Ingarao G, Lunetto V et al (2018) The role of re-design for additive manufacturing on the process environmental performance. Procedia CIRP 69:124–129. https://doi.org/10.1016/j.procir.2017.11.047
23. Mecheter A, Tarlochan F, Kucukvar M (2023) A review of conventional versus additive manufacturing for metals: life-cycle environmental and economic analysis. Sustainability 15:12299. https://doi.org/10.3390/su151612299
24. Serres N, Tidu D, Sankare S, Hlawka F (2011) Environmental comparison of MESO-CLAD® process and conventional machining implementing life cycle assessment. J Clean Prod 19:1117–1124. https://doi.org/10.1016/j.jclepro.2010.12.010
25. Priarone PC, Ingarao G (2017) Towards criteria for sustainable process selection: on the modelling of pure subtractive versus additive/subtractive integrated manufacturing approaches. J Clean Prod 144:57–68. https://doi.org/10.1016/j.jclepro.2016.12.165
26. Morrow WR, Qi H, Kim I et al (2007) Environmental aspects of laser-based and conventional tool and die manufacturing. J Clean Prod 15:932–943. https://doi.org/10.1016/j.jclepro.2005.11.030
27. Nagalingam AP, Shamir M, Tureyen EB et al (2025) Recent progress in wire-arc and wire-laser directed energy deposition (DED)

of titanium and aluminium alloys. Int J Adv Manuf Technol 136:2035–2073. https://doi.org/10.1007/s00170-024-14967-w
28. Williams SW, Martina F, Addison AC et al (2016) Wire + arc additive manufacturing. Mater Sci Technol 32:641–647. https://doi.org/10.1179/1743284715Y.0000000073
29. Bermingham MJ, Nicastro L, Kent D et al (2018) Optimising the mechanical properties of Ti-6Al-4V components produced by wire + arc additive manufacturing with post-process heat treatments. J Alloys Compd 753:247–255. https://doi.org/10.1016/j.jallcom.2018.04.158
30. ANSYS Inc. (2025) ANSYS Granta Selector: materials data and selection software, Version 2025 R1. Canonsburg, PA, USA
31. Hammond G, Jones C (2010) Inventory of Carbon and Energy (ICE), Annex B: How to Account for Recycling a Methodology for Recycling. The University of Bath, Bath, UK
32. Gobber FS, Priarone PC, Pennacchio A, Actis Grande M (2024) Effect of inert gas pressure on the properties and carbon footprint of UNS S32760 powders made from waste materials by gas atomization. J Mater Res Technol 33:8814–8828. https://doi.org/10.1016/j.jmrt.2024.11.195
33. European Environment Agency (EEA) (2025) Greenhouse gas emission intensity of electricity generation in Europe. Available via European Environment Agency. https://www.eea.europa.eu/en/analysis/indicators/greenhouse-gas-emission-intensity-of-1. Accessed 24 Sep 2025
34. International Energy Agency (IEA) (2025) Electric power transmission and distribution losses (% of output). Available via World Bank Open Data. https://data.worldbank.org/indicator/EG.ELC.LOSS.ZS. Accessed 24 Sep 2025
35. Catalano AR, Pagone E, Martina F et al (2023) Wire arc additive manufacturing of Ti-6Al-4V components: the effects of the deposition rate on the cradle-to-gate economic and environmental performance. Procedia CIRP 116:269–274. https://doi.org/10.1016/j.procir.2023.02.046
36. Dias M, Pragana JPM, Ferreira B et al (2022) Economic and environmental potential of wire-arc additive manufacturing. Sustainability 14:5197. https://doi.org/10.3390/su14095197
37. Catalano AR, Tebaldo V, Priarone PC et al (2025) CMT deposition of stainless steel: effects of process parameters on energy demand and microstructure. Prog Addit Manuf 10:6993–7013. https://doi.org/10.1007/s40964-025-01022-7
38. Fuchs C, Baier D, Semm T, Zaeh MF (2020) Determining the machining allowance for WAAM parts. Prod Eng Res Devel 14:629–637. https://doi.org/10.1007/s11740-020-00982-9
39. Thien A, Saldana C, Kurfess T (2022) The effect of WAAM process parameters on process conditions and production metrics in the fabrication of single-pass multi-layer wall artifacts. Int J Adv Manuf Technol 119:531–547. https://doi.org/10.1007/s00170-021-08266-x
40. Catalano AR, Priarone PC, Settineri L (2024) An economic evaluation of hybrid WAAM-subtractive manufacturing in relation to deposition process parameters. Procedia CIRP 122:49–54. https://doi.org/10.1016/j.procir.2024.02.003
41. Babu A, Trodini E, Argumedo JLG et al (2025) Correlating geometry, microstructure and properties of high strength steel thin wall structures fabricated with WAAM. J Adv Join Process 11:100292. https://doi.org/10.1016/j.jajp.2025.100292
42. Geng H, Li J, Xiong J et al (2018) Formation and improvement of surface waviness for additive manufacturing 5A06 aluminium alloy component with GTAW system. Rapid Prototyp J 24:342–350. https://doi.org/10.1108/rpj-04-2016-0064
43. Duarte V, Rodrigues T, Schell N et al (2021) Wire and arc additive manufacturing of high-strength low-alloy steel: microstructure and mechanical properties. Adv Eng Mater 23:2001036. https://doi.org/10.1002/adem.202001036
44. Chernovol N, Sharma A, Tjahjowidodo T et al (2021) Machinability of wire and arc additive manufactured components. CIRP J Manuf Sci Technol 35:379–389. https://doi.org/10.1016/j.cirpj.2021.06.022
45. Fonseca PP, Duarte VR, Farias FWC et al (2025) Enhancing manufacturing and post-processing properties of WAAM ER110 HSLA steel: in situ hot forging + post-deposited heat treatment effects on surface quality and specific cutting energy. Prog Addit Manuf 10:3417–3436. https://doi.org/10.1007/s40964-024-00814-7
46. Rodriguez N, Vázquez L, Huarte I et al (2018) Wire and arc additive manufacturing: a comparison between CMT and TopTIG processes applied to stainless steel. Weld World 62:1083–1096. https://doi.org/10.1007/s40194-018-0606-6
47. Rodrigues TA, Duarte V, Miranda RM et al (2019) Current status and perspectives on wire and arc additive manufacturing (WAAM). Materials 12:1121. https://doi.org/10.3390/ma12071121
48. Li F, Chen S, Shi J et al (2018) Thermoelectric cooling-aided bead geometry regulation in wire and arc-based additive manufacturing of thin-walled structures. Appl Sci 8:207. https://doi.org/10.3390/app8020207
49. Frank M, Harrysson O, Wysk R, et al (2017) A Method for Integrating Additive and Subtractive Operations for Metal Parts – Direct Additive Subtractive Hybrid Manufacturing (DASH). In: Materials Science & Technology 2017 Conference Proceedings. pp 366–368. https://doi.org/10.7449/2017/mst_2017_366_368
50. Ashby MF (2013) Materials and the environment: eco-informed material choice, 2nd edn. Elsevier/Butterworth-Heinemann, Amsterdam. https://doi.org/10.1016/C2010-0-66554-0

Publisher's Note Springer Nature remains neutral with regard to jurisdictional claims in published maps and institutional affiliations.